19

Laser Altimetry: What Can Be Learned About Geology and Surface Processes from Detailed Topography

Tim Webster
Applied Geomatics Research Group
Nova Scotia Community College, Middleton, Canada

1. Introduction

Earth Science has utilized new remote sensing techniques for many years, weather it be airborne geophysics to sense the magnetic field or aerial photography and satellite imagery to obtain that ever important synoptic view that aids in our interpretation of the landscape and geology. The field of geomatics, which is the acquisition, analysis and mapping of the earth's surface, has emerged and drives the commonplace web applications like Google maps and Google earth. Geomatics is important in the earth science sector for many areas including: utilizing global positioning systems (GPS) for locating their property, infrastucture and geological samples, a geophysical-image analysis system for analyzing and display of their remote sensing data from geophysical (seismic, radiometric isotopes, electromagnetic, etc.) to imagery (airphotos, satellite) data, and a geographic information system (GIS) to house all of these data in addition to other geospatial data (points: wells, sample assays, etc.; lines: roads, streams, contours, etc.; and polygon: claim block, watershed, anomalies, etc.) and raster or grid cell based maps. Landscapes are influenced by several factors including geology, soils, climate, glaciations, topography, and vegetation cover, among others. In order to study geology and the influence on landscapes and their evolution, we attempt to map these different factors using geomatics.

2. Digital elevation models – lidar

One of the most critical layers to describe a landscape is the topography of the terrain, which is expressed as a digital elevation model (DEM) within a GIS environment. Most elevation models have been derived from stereo aerial photography, in which measurements of the ground are hampered by the tree canopy. The challenge to make accurate topographic measurements of the earth under the forest canopy has been a problem until recently. Airborne laser scanning has the ability to solve this problem and see through the vegetation, depending on the canopy density and closure. Light Detection and Ranging (lidar) is a technique that combines a laser ranging system with an inertial navigation system comprised of a survey grade GPS and an inertial measurement unit (IMU) in an aircraft (Fig. 1). Detailed technical overviews of lidar systems have been described by various authors (Flood et al., 1997; Gomes Pereira and Wicherson, 1999; When and Lohn, 1999; and Maune,

2001). Lidar has been used in a number of geoscience applications, including the analysis of river networks (Stock et al., 2005), the generation of cross-sections across rivers (Charlton et al., 2003), in general glaciology (Krabill et al., 1995, 2000), groundwater monitoring (Harding and Berghoff, 2000), investigation of landslides (McKean and Roering, 2003), and in the mapping of tectonic fault scarps and geomorphic features (Haugerud et al., 2003) and examining coastal processes (Brock et al., 2002). Lidar has been used to demonstrate improvements in mapping bedrock and surfical geology as well as landscape metrics such as stream incision, and to resolve and map the individual volcanic flow units of the North Mountain Basalt and the identification of crater structures within the lower flow unit (Webster et al., 2006, 2006 A). Lidar has been merged with geophysical data to revise the geological boundaries along the Avalon-Meguma terrain boundary in Nova Scotia, Canada (Webster, Murphy and Quinn, 2009). Webster et al. (2009) used lidar and drill logs to estimate the thickness of aggregate deposits in the Annapolis Valley, NS.

The detail and resolution of DEMs derived from lidar are ten times better than previous available data for these areas. Generally, DEMs derived from aerial photography or other remote sensing systems such as the Shuttle Radar Topography Mission (SRTM) have degraded accuracies in forested areas and have horizontal resolutions of ca. 20 – 30 m. The benefit of lidar is that a narrow laser beam is directed from the aircraft towards the earth's surface and reflected back in order to measure the range or distance from the aircraft to the ground. The beam divergence is typically very small (0.3 rmad), resulting in a laser footprint diameter of 30 cm on the ground at 1000 m flying height. The system is mounted in an aircraft and the laser fires hundreds of thousands of shots per second that are directed across a swath toward the earth's surface by an oscillating mirror (Fig. 1).

The laser pulse is reflected back to the sensor, which records the two-way travel time that is then converted into a range or distance based on the speed of light (Fig. 1). Since the laser pulse can partially hit several targets (top of canopy, branches, tree trunk, buildings, shrubs, and ground) the lidar sensor can record several returns. Earlier Lidar sensors, ca 2003, could record a single return, first or last. Today's sensors are capable of capturing multiple returns, for example the Optech ALTM-3100 model is capable of recording up to four returns per emitted pulse. For many surveys there is no requirement for these intermediate laser returns so only the first and last returns are recorded during the survey. The laser range distances are combined with the angular and trajectory data from the scan mirror, GPS and IMU to determine the three-dimensional location of the targets in the GPS World Geodetic System of 1984 (WGS84) mapping system. A local GPS base station is setup over a known monument to establish geodetic control for the survey (Fig. 1). Ground check points should also be acquired along road surfaces within the survey area in order to validate the lidar elevations as part of the vertical accuracy assessment process. The GPS from the aircraft (rover) is combined with that of the base station (reference) in order to obtain the position of the aircraft every second. The GPS information is combined with the angular measurements from the IMU that are 200 times per second (Fig 1). The lidar points are generally output to a map projection coordinate system, typically Universal Transverse Mercator (UTM) in meters east and north. The lidar elevations are referenced to the GRS80 ellipsoid and not above mean sea level or a local national vertical datum. A geoid-ellipsoid model can be used to convert the elevations from ellipsoidal to orthometric heights above the geoid. In Canada we currently use the HT_2 model supplied by the Canadian Geodetic Survey of Natural Resources Canada to relate ellipsoidal heights to the Canadian Geodetic Vertical Datum of 1928 (CGVD28). The lidar surveys are typically acquired in swaths along overlapping flight lines or strips (Fig. 2).

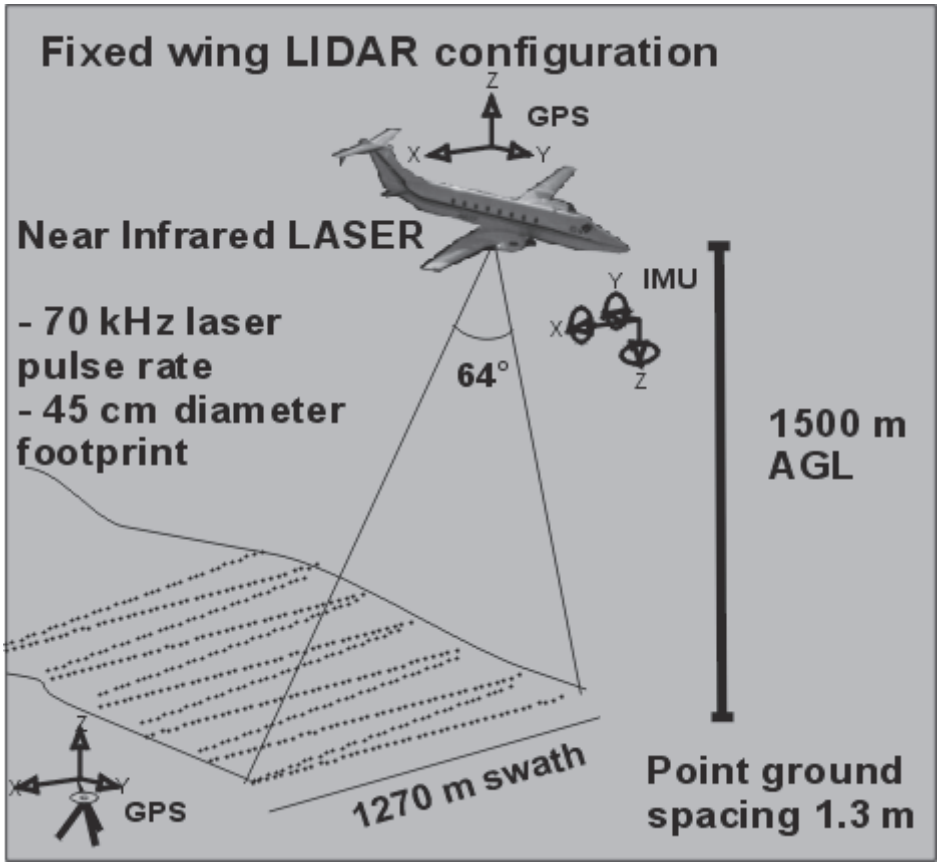

Fig. 1. Typical wide area lidar survey configuration. The laser firing at 70 kHz, with the pulses directed across the swath at 25 Hz at a height of 1500 m.

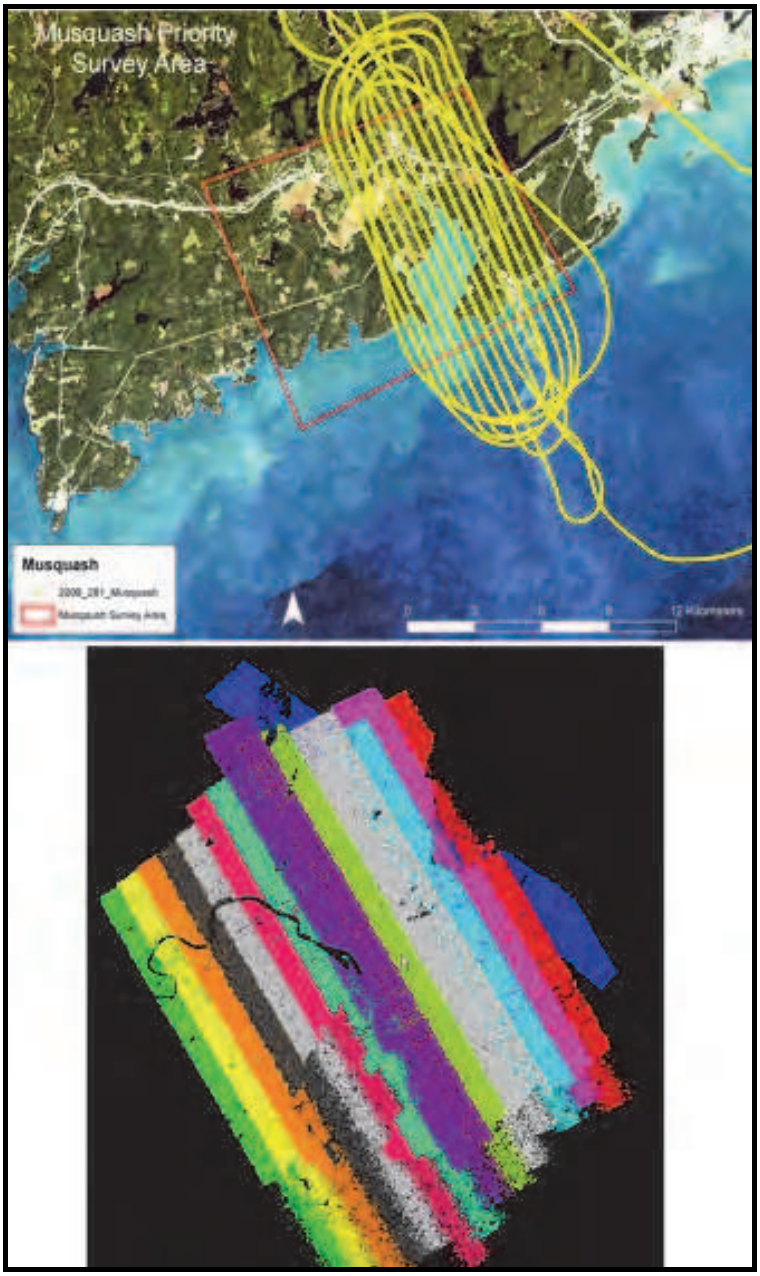

Fig. 2. Top map shows the flight trajectory of the aircraft during a lidar survey, yellow dots. The bottom map shows the lidar swaths associated with the above flight lines. Note the black outline of the river where no returns were detected because of the smooth mirror like surface of the water. Musquash, New Brunswick, Canada.

The trajectory is solved from the blend of GPS and IMU data to position the aircraft, then the laser ranges and scan mirror angles are used to compute the target position in space. The results are a set of high-density points known as a 'point cloud' that represent the ground and other targets, such as vegetation or anthropogenic features e.g. roads, buildings, bridges (Fig. 3).

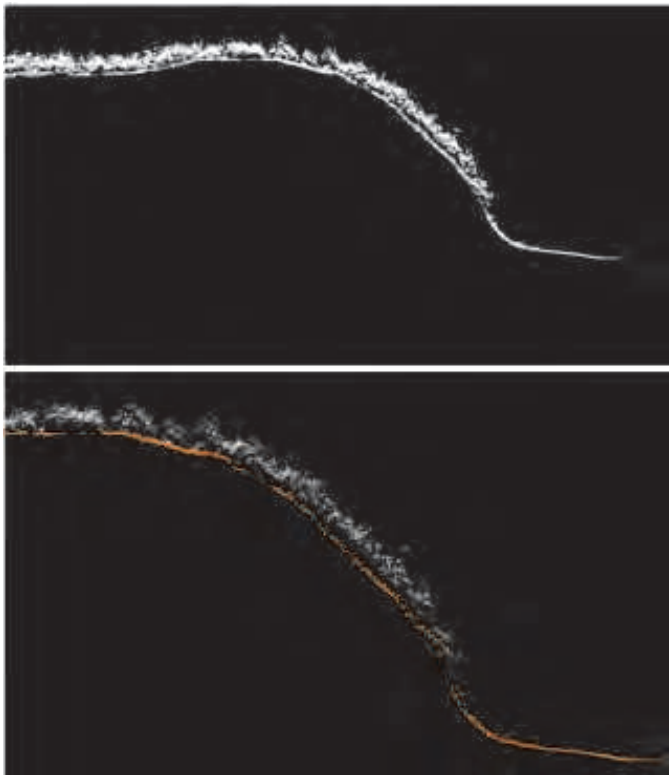

Fig. 3. Cross section of a lidar point cloud along a coastal area. Top cross-section of unclassified points. Bottom cross-section of classified ground points in orange. The remaining points are vegetation.

In order to derive an accurate DEM, the lidar points are classified or filtered into 'ground' and 'non-ground' target classes (Fig. 3). The point cloud is classified using specialized software where the points for each strip are merged together and broken down into a series of tiles based on a map projection grid system and processed individually. The classification algorithms can have problems producing accurate results in rough terrain or discontinuous slopes, dense forest areas where the beam cannot penetrate to the ground, and low vegetation being confused with the ground. Generally the lowest points are used to construct an initial surface from a Triangular Irregular Network (TIN). Then each additional point is added to the TIN if the parameters are below the threshold settings. The problem is that different thresholds are required for different terrain conditions. The two sets of lidar points, 'ground' and 'non-ground' are integrated into a GIS that can be used to interpolate different types of surfaces from the combination of points. Surfaces, such as a Digital Surface

Model (DSM) by using all of the lidar points (including those representing vegetation and ground) and the DEM using only the 'ground' points are constructed using the interpolation routines (Fig. 4). In addition to recording the time of the near-infrared 1064 nm laser pulse, the lidar system also records the amplitude of the returning pulse, known as the intensity. The intensity will vary depending on the material of the target; low reflective materials like asphalt will have very little energy returned and a low intensity compared to grass which will have a high intensity. The intensity of the points are interpolated to form a black and white type of photograph, since all of the points are used we refer to it as DSM intensity or DSMI (Fig. 4). Because the DSMI is grey-scale and is related to land cover rather than elevation, it can be combined with the DEM and DSM to form a hybrid image (Fig.4). The manipulation of lidar surface models in a GIS allows for the construction of maps that can preferentially highlight subtle geomorphic features (e.g. artificial sun illumination and vertical exaggeration). Such features are often not readily observed in traditional DEMs, or from stereoscopic inspection of aerial photographs, because of their low relief and obstructions from vegetation. Because of the scale of the many geological features being studied, regional-scale lidar surveys are required in order to assess its applicability to geomorphic research, such that features with a topographic expression can be detected and traced over long distances.

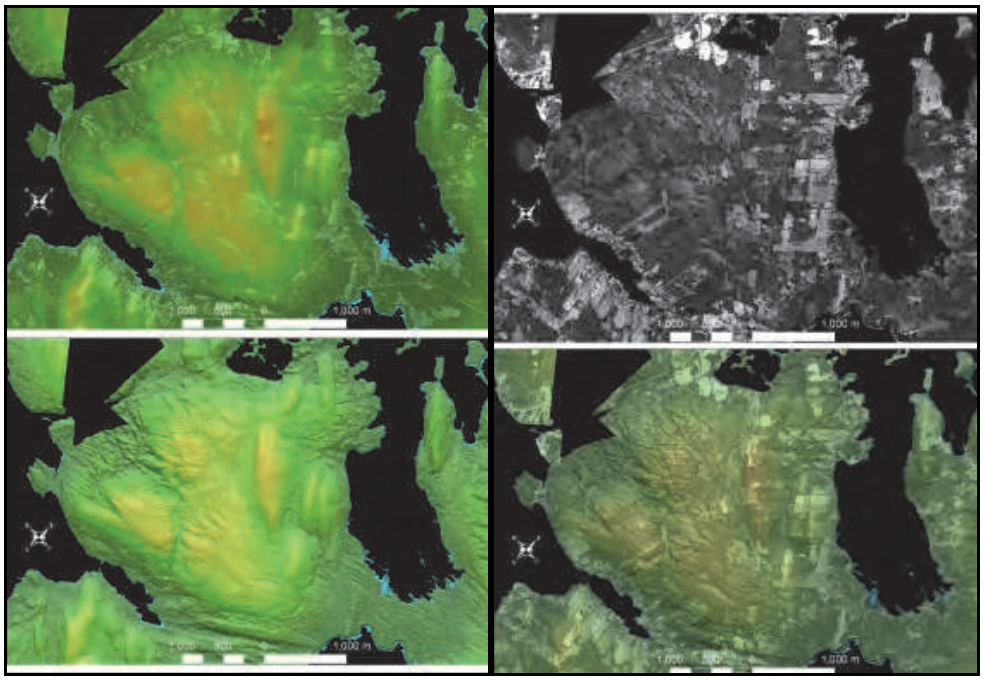

Fig. 4. Lidar surface models: Upper left map - Digital Surface model DSM using all the lidar points; Lower right map is a Digital Elevation Model DEM of ground only points; Upper Right map is the grey scale lidar intensity (land cover); Lower right map is the hybrid of the intensity plus the DEM. The folds and faults in the bedrock and drumlins are visible in the 2nd map of the DEM. Riverport, Nova Scotia, Canada.

3. Visualization

Grey-scale shaded relief maps can be constructed by illuminating the DEM from azimuth angles to highlight topographic features which trend in the perpendicular direction, for example if a topographic high trends east-west, then an illumination azimuth angle of 0 or 180 degrees would highlight the features. In addition to an azimuth illumination angle, a zenith angle can be expressed to denote where the light source is in the sky relative to the horizon. The cartographic convention for shaded relief maps is to illuminate the terrain (DEM) from the northwest or 315 degrees and with a zenith angle of 45 degrees. In order to enhance the terrain and have enough contrast between bright and darker surfaces, depending on the relief of the study area, a vertical exaggeration can be applied. A lidar DEM has been processed for a section of the Annapolis Valley, Nova Scotia and used to demonstrate various processing techniques. In the following example, the DEM has been illuminated from the eight cardinal directions 0, 45, 90, 135, 180, 225, 270 and 315 degrees at a constant zenith angle of 45 degrees and a 5 time vertical exaggeration applied (Fig. 5). The resultant grey-scale images reveal the texture or relief of the terrain, however they do not indicate the absolute elevation of features, for example a sloping surface will look the same regardless of the absolute elevation. By illuminating the terrain from different azimuth angles, different topographic features are revealed, depending on their orientation (Fig. 5). The ability to vary the sun angle and apply a vertical exaggeration is very useful in geology to enhance subtle topographic features such as lineaments, contact ridges or surficial deposits. These maps reveal two distinct morphological characteristics of the terrain with respect to the roughness of the topography. Some areas of the terrain are rough and ridges represent different volcanic flow units in contrast to smoother sections that represent areas that have a glacial till blanket covering the bedrock (Fig 5). This reflects differences in glacial history; areas to the west consist of glacially scoured bedrock with a thin till veneer, and areas to the east have a thick blanket of glacial till, known locally as the Lawrencetown Till (LT) (Stea and Kennedy, 1998). Since the shading of the terrain is limited to one direction, the resultant map only highlights features perpendicular to the shading direction and subdues features parallel to it. The application of principal components analysis, which is used to reduce data redundancy and compress multi-channel information into fewer components, has been used on multiple Radatsat images by Paganelli et al. (2003) for structural mapping. When PCA is applied to the 8 shaded relief maps, a new map is constructed where the top three principal components contain over 98% of the information, or the original variance of the 8 maps (Fig. 6). The three components PCA 1,2,3 are projected through the red, green and blue colour guns to form the new composite that highlights all of the topographic features, regardless of their orientation. The advantage of this map, in contrast to the grey-scale images, is that very few areas are in shadow and more features are highlighted (Fig. 6). The composite may be difficult to interpret since it reflects the dominant topographic features of the landscape in the 3 components. The dominant landforms are the North and South Mountains, highlighted in shades of red, separated by the Annapolis Valley in shades of green. The topographic feature which face southeast are in shades of blue (Fig. 6). In addition to the PCA composite the mapped surficial geology deposits of the Lawrencetown Till blanket (TL) have also been superimposed to compare to the terrain roughness. The arrow in figure 6 denotes a change in the glacial landforms visible in the valley. To the west of the arrow, the landforms resemble drumlins associated with an earlier ice movement. To the east of the arrow, streamline landforms are visible in the valley that represents the last movement of ice (Fig. 6). The black box in figure 6 denotes areas where raised beach terraces are visible on the DEM.

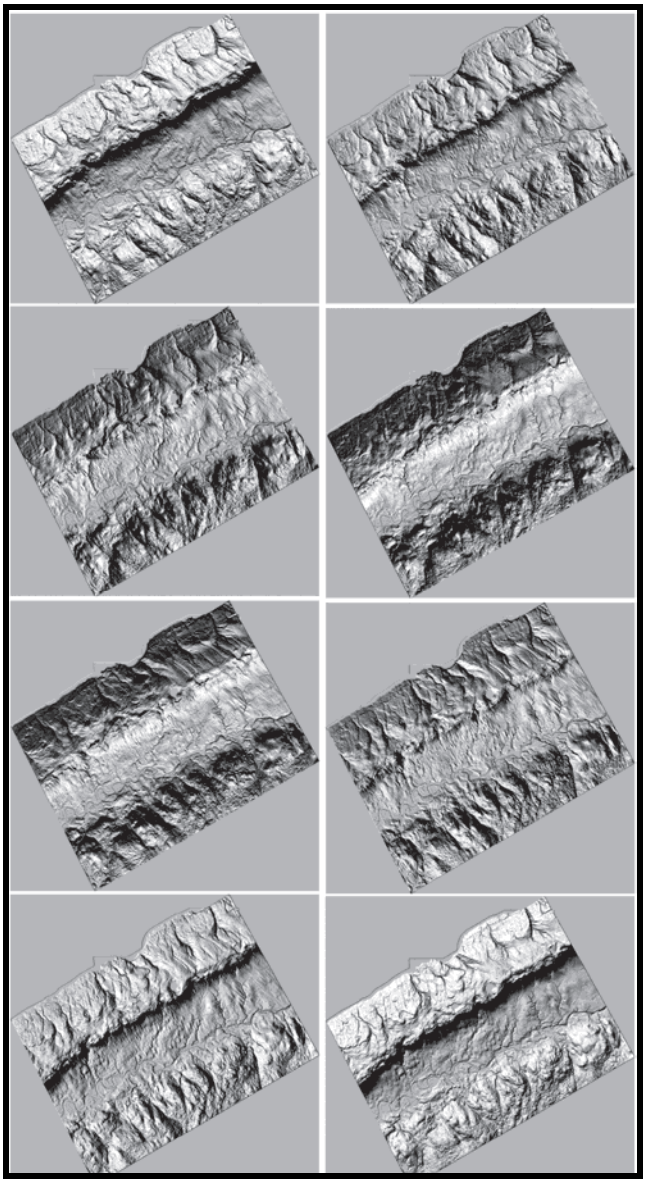

Fig. 5. Shaded relief maps on a lidar DEM for a section of the Annapolis Valley, Nova Scotia. All maps have had a zenith angle of 45 degrees and a vertical exaggeration of 5 times aplied. Top left azimuth of 0 degrees, top right azimuth of 45 degrees, second row left azimuth of 90 degrees, second row right azimuth of 135 degrees, third row left azimuth of 180 degrees, third row right azimuth of 225 degrees, bottom row left azimuth of 270 degrees, and bottom row right azimuth of 315 degrees. Images are approximately 15 km by 10 km. North is at the top of the page.

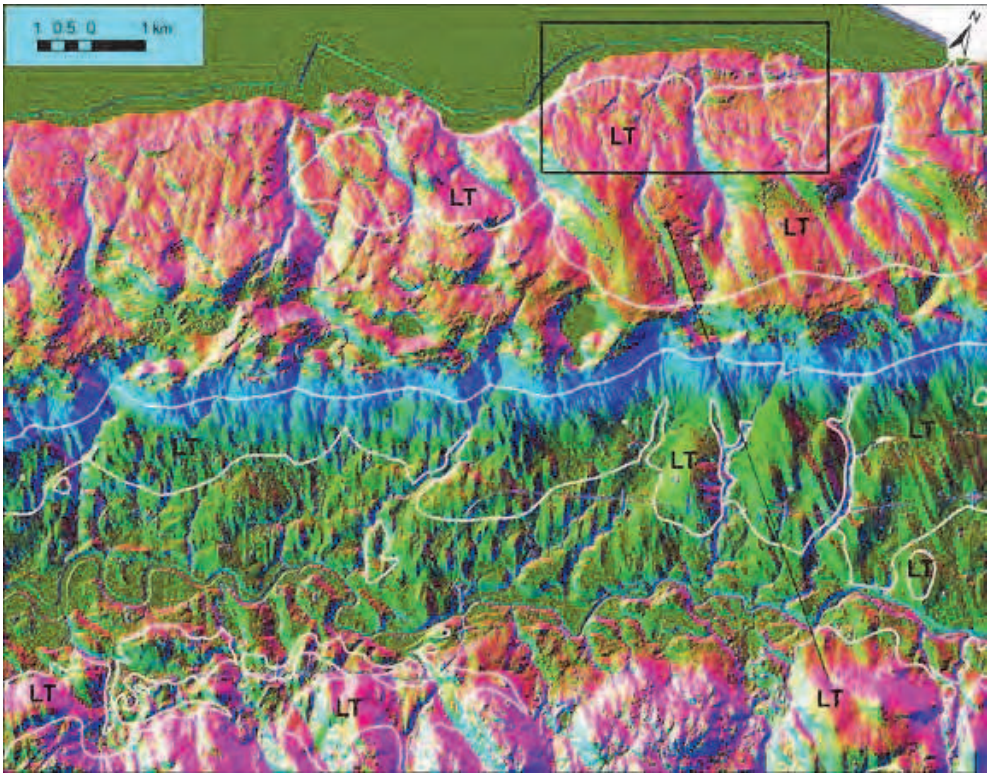

Fig. 6. Principal components 1,2,3 in red, green, blue respectively from the eight shaded relief maps (Fig. 5). The white outline represents the surficial geology boundaries of the Lawrencetown Till blanket (LT).

Another common method to enhance DEM for visualization is to construct a colour shaded relief model (CSR). This has the advantage of the shading enhancing the texture of the topography and the hypsometric colours denoting the absolute elevation of the terrain. An example of a CSR map for this area was constructed by first building a grey scale shaded relief map, with the sun illumination from the northwest (335^{o}) at a zenith angle of 45^{o} with a 5-times vertical exaggeration, then colour was applied to the DEM based on elevation, from below sea-level (hues of blue), to low lying land (green through yellow) to the highest point along the North Mountain (ca 265 m) (red) (Fig. 7). The colourized DEM is then merged with the grey scale shaded relief map in order to provide the texture of the terrain as a result of the shading effect. Since the colours have been applied to the terrain from the lowest elevation corresponding to the shortest visible wavelength (blue) to the highest elevation corresponding to the longest visible wavelength (red), the map appears in 3-D if viewed with Chromadepth™ glasses. Chroma stereoscopy is the technique of using colour to depict depth (Toutin and Rivard, 1995). The glasses are based on a diffraction grating which separates the incident light into different patterns depending on the wavelength. Since the map is coded from low to high elevation by low to high wavelengths of light we see depth when the brain is forced to fuse the multiple image patterns together to form a

single image of the terrain. The benefit of this technique is that that map can be viewed and interpreted with or without the 3-D glasses. In comparison to the anaglyph method that requires the red and blue glasses to reveal a 3-D image in black and white. This technique offsets each image in red and blue proportional to the elevation; however, the map only can be easily interpreted when it is viewed with the glasses.

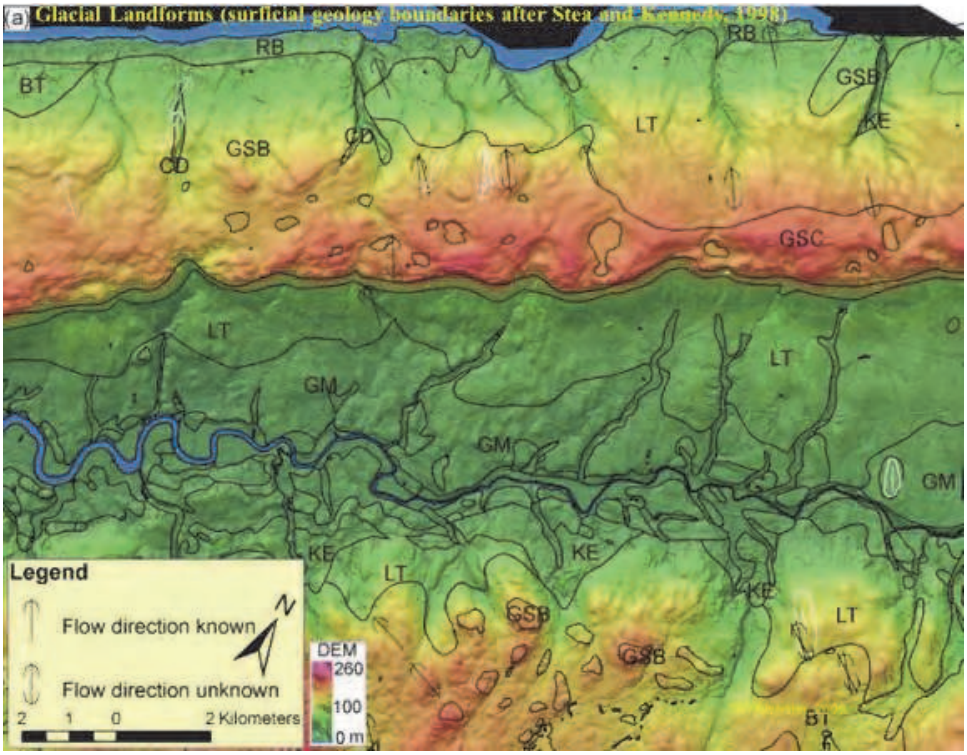

Fig. 7. Colour shaded relief map from lidar DEM. Surficial geological boundaries have been superimposed. The colour scheme is optimized for a Chroma-stereoscopic affect when viewed with 3-D Chromadepth™ glasses.

This technique of merging a grey-scale image with a colour image has been utilized in the past to integrate geophysical data with radar imagery or lidar shaded relief maps (Webster, Murphy and Quinn, 2009). It has also been used to generate "pan sharpened" images utilizing the new optical satellites where a panchromatic band at a 0.5 m resolution is combined with a multispectral (colour) set of bands at a courser resolution such as 2.5 m. The resultant hybrid image has the benefits of the 0.5 m panchromatic detail and the spectral colour information of the courser dataset. In geoscience, this method of data integration is especially useful when datasets that provide complimentary information that can be interpreted when they are integrated. For example, the lidar DEM highlights variations on the surface topography that reflects both bedrock and surficial geology features. Airborne radiometric surveys measure the amount of equivalent uranium, thorium and percent potassium near the surface and have been used in exploration. Since the gamma rays that the

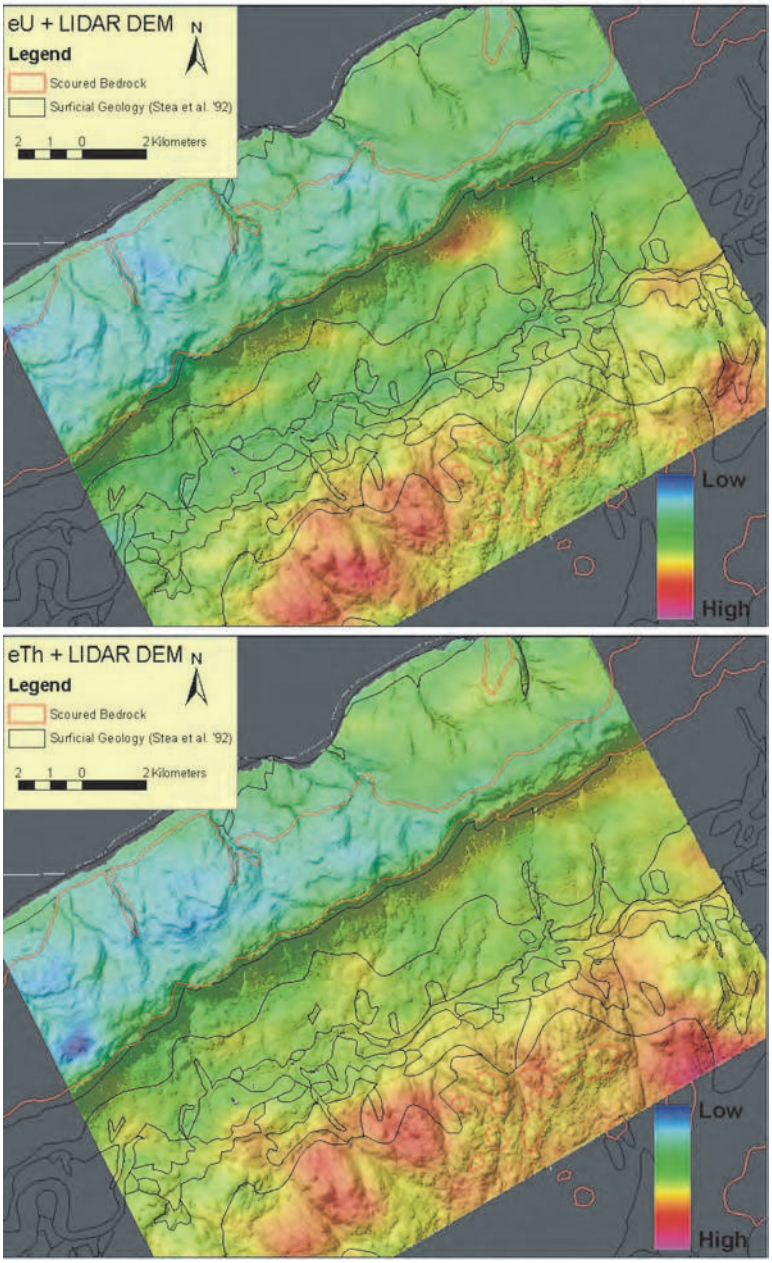

Fig. 8. Radiometric equivalent uranium (top) and thorium (bottom) have been colourized and merged with the lidar shaded relief maps. Low concentrations are colour coded blue through higher concentrations in red. The red areas on the south side of the valley correspond with granite bedrock.

sensor detects do not penetrate vary far through the soil, this geophysical measurement indicates what the concentration of the radioactive isotopes is near the surface. These airborne surveys are often gridded at a course resolution, ca. 250 m where the features appear blurry compared to the detail of lidar maps. The shaded relief lidar has been merged with the colourized equivalent uranium and thorium to produce hydrid maps (Fig. 8). The surficial geology boundaries have been superimposed which indicate the glacial till has a different radiometric signature that the underlying bedrock geology of the North Mountain (Fig. 8). The glacial till contains fragments of the South Mountain Batholith granite which occurs on the south side of the valley (MacDonald and Ham, 1994). The boundary between the scoured glacial bedrock (red outline) and the glacial Lawrencetown Till (Fig. 6-7) is highlighted by the contrast in radiometric element concentrations. The thorium values are anomalously low in the area of a crater within the basalt flow units and may reflect a difference in the chemistry of the basalt in that location (Fig 8 bottom). This technique allows two datasets to be interpreted at the same time and for the courser resolution dataset to be sharpened based on the detail of the grey-scale data. GIS systems allow the user to "fly through' the data or generate perspective views of the terrain and drape other GIS layers, either in the form of imagery or maps on the terrain. This technique further enables us to interpret the terrain and the relationship to lithology or glacial history. The ability to quickly visualize the terrain in a perspective view can often reveal relationships that are not readily visible from the standard top down map view (Fig. 9).

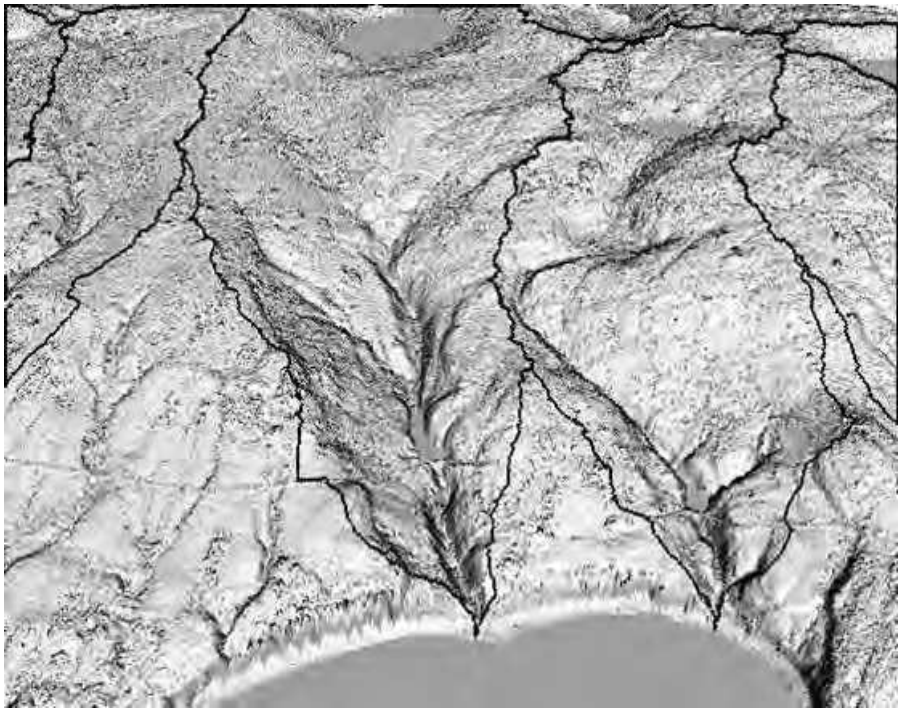

Fig. 9. Perspective view of shaded relief lidar map with the watershed boundaries superimposed.

4. Modern day processes: Watersheds and erosion

Understanding the relationship between stream incision and factors related to fluvial erosion such as rock-uplift, climate, base level changes, and bedrock resistance to erosion (e.g. Stock and Montgomery, 1999; Kirby and Whipple, 2001; Stock et al., 2005) is important for the analysis of landscape evolution (e.g. Kooi and Beaumont, 1996; Dietrich et al., 2003; Pazzaglia, 2003). The availability of high resolution lidar DEMs can facilitate quantitative analysis between incision and watershed morphometrics at sufficiently small scales to allow the examination of isolated influences on stream evolution. Previous studies have considered the relationship between the variations in the resistance of bedrock to erosion (Sklar and Dietrich, 2001) and stream or basin morphometry to the fluvial processes between regions (Belt and Paxton, 2005). However, the variations of bedrock resistance within a region (< 100 km^2) are less constrained, in part due to the scale of studies (Montgomery and Lopez-Blanco, 2003).

Fluvial processes in glaciated terrain are complex because glaciers and streams sequentially may occupy the same valleys but obey different laws of erosion, making the signatures of glacial and fluvial processes difficult to distinguish. Studies applying the stream power law often use the contributing drainage area as a surrogate parameter for stream discharge which, in addition to the local channel slope, controls the stream's ability to incise the underlying bed (e.g. Snyder et al., 2000). However, few studies examine the local hydrological effects of surface and groundwater interaction on discharge (Tague and Grant, 2004). At this scale, factors such as glacial till cover and the fracture density of bedrock can influence infiltration rates and affect peak annual stream discharge.

An example of utilizing a high-resolution lidar DEM to examine metrics of similarly-sized catchments that have been modified by glaciation is presented for the North Mountain within the Fundy Basin. The study area was selected because (i) the catchments are developed on three shallowly dipping volcanic flow units of the Jurassic North Mountain Basalt (NMB) which each have uniform resistance to erosion throughout the study area, (ii) the Bay of Fundy provides a uniform base level for all streams, (iii) there is a clear distinction in till cover thickness over the east and west portions of the study area, and (iv) the age of deglaciation and subsequent fluvial erosion is well documented and uniform throughout. The stream incision depths are related to the variability of the flow unit's resistance to erosion.

The land cover on the North Mountain is influenced by the occurrence of the till cover; farmland (pastures and hayfields) and mixed forest dominate in the east where the till is thickest, whereas the west has mostly mixed forest cover. There are more roads and anthropogenic influences in the east compared to the west where only one paved road occurs along the coast. The coastline varies between gently sloping bedrock platforms and ca. 25 m cliffs that occur in embayments. The streams on the Fundy side of NMB have evenly-spaced mainstems (1.5 km), similar catchment areas (ranging from 2 to 8 km^2) and are all consequent dendritic drainages with stream densities ranging from 0.9 to 2.9 km/km^2. The streambeds are typically 80% bedrock and 20% boulder-covered. Till is present in the streambed of some of the basins, attesting to the youthfulness of these catchments and to the inheritance of some low relief pre-glacial topography. Within the NMB study area, there are similar size basins (2 – 8 km^2) that drain scoured bedrock, and occur in the transition zone with scoured bedrock in their headwaters and glacial till near their outlets, and drain a glacial till blanket covering the basalt. The streams are ephemeral with their peak flows occurring in the spring and fall seasons. Their long profiles are ungraded and have several knick zones.

Watersheds are calculated for the main streams draining into the Bay of Fundy from the lidar DEM based on outlet locations identified on 1:10,000 scale topographic maps (Fig. 10). Most GIS systems can calculate the watershed draining into a stream based on the DEM. The standard D-8 algorithm (Jenson and Dominque, 1988; Costa-Cabral and Burges, 1994) is used to determine down-stream flow direction and sinks (depressions within the DEM treated as errors by the algorithm) are filled in the DEM to allow continuous down stream flow. However, when dealing with DEMs at high-resolution, other considerations must be made. Inspection of the drainage basin boundaries and stream longitudinal profiles indicates that most catchments have sinks. Many of these sinks are adjacent to the raised elevations of a roadbed captured by the high resolution of the lidar. As a culvert could not be represented on the DEM, a "notch" was cut across the roadbed and assigned an elevation of the nearest downstream cell to improve the accuracy of the flow direction algorithm and to prevent excessive erroneous sink filling operations in deriving the catchment basins and stream profiles. This modification improved accuracy of the flow direction algorithm, prevented excessive erroneous sink-filling operations in deriving the catchment basins and stream profiles, and allowed the stream to "pass through the roadbed". The overall result is the generation of a more accurate flow accumulation grid and basin boundary (Fig. 9-10). It

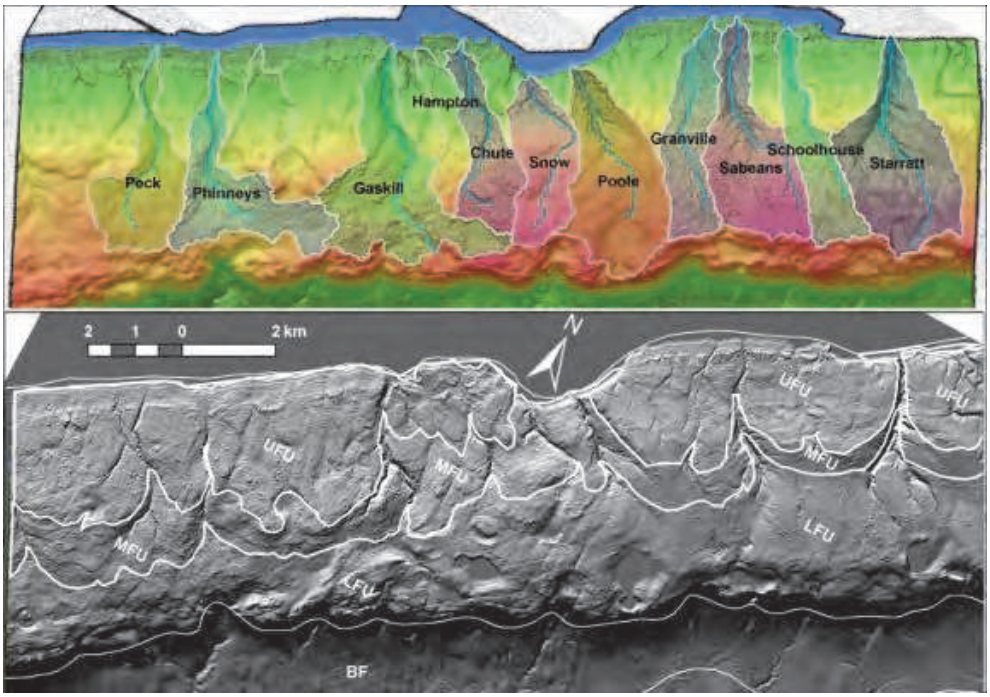

Fig. 10. Top: Lidar DEM with derived watershed boundaries for the streams draining the North Mountain Basalt. Bottom: Basalt flow units for the North Mountain over grey-scale shaded relief lidar DEM. UFU – Upper Flow Unit, MFU – Middle Flow Unit, LFU – Lower Flow Unit.

was determined that the streams from the topographic map and the longitudinal profiles obtained from the original DEM prior to sinks being filled are the most representative based on field observation and used for analysis. The flow units of the NMB have been subdivided into three distinct flow units: the lower flow unit (LFU) consists of a thick (40 - 150 m) massive single flow that is columnar jointed, the middle flow unit (MFU) conformably overlies the LFU, and consists of multiple thin flows that are highly vesicular and amygdaloidal, and the upper flow unit (UFU) conformably overlies the MFU, outcrops along the shore, and consists of 1-2 massive flows (Fig. 10 bottom).
The surface profiles of the drainage divides bordering each basin are averaged and the stream longitudinal profile is subtracted to compute the incision depth along the stream's entire length. The basalt flow units were intersected with the stream longitudinal profiles and the incision depth was summarized for each flow unit (Fig. 11).

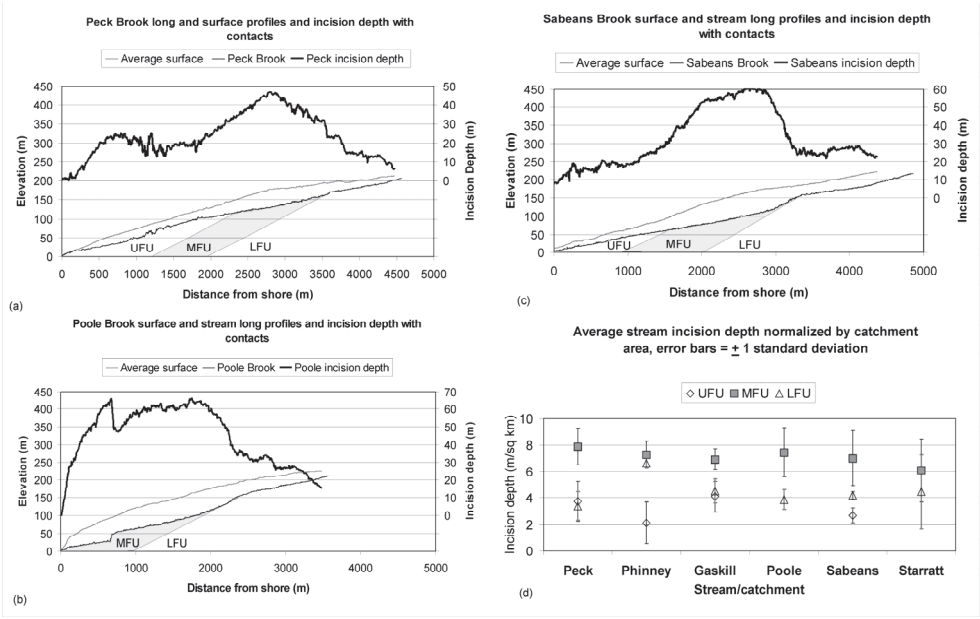

Fig. 11. Stream incision depth diagrams for the main drainage basins along the North Mountain. The surface profiles associated with the drainage divides and the stream long profile are plotted along with the depth of incision (difference between surface and stream profiles). The NMB flow unit (UFU, MFU, LFU) contacts have also been projected to intersection the streambed and related to the depth of incision. (A) Peck Brook profiles and incision. (B) Poole Brook profiles and incision. (C) Sabeans Brook profiles and incision. (D) Average incision depth for each flow unit of the NMB normalized by the drainage area for each basin and error bars indicates ± 1σ.

The stream profiles and incision depths were overlain on the flow unit map of the NMB in order to relate the incision depth to the basalt flow units. The flow units dip approximately 6° to the northwest and have been projected onto the stream profiles (Fig. 11). In general the stream incision depth reaches a maximum within the middle flow unit (MFU). Many knick

zones occur either within the MFU or upstream of the contact between the MFU and lower flow unit (LFU). Incision in the upper flow unit (UFU) and LFU is similar in 3 of the 4 basins studied where both units outcrop in the streambed (Fig. 11, D). The average incision depth for the MFU is 45 m compared to 29 and 19 m for the LFU and UFU, respectively. The area percentage of each flow unit per basin and the length percentage of each flow unit per stream suggest that the percentage of flow unit per basin is a better indicator of stream incision depth than the percentage of stream length within a flow unit. The average incision depth is lowest in the catchments where the till cover is thinnest. However, the highest incision depths are associated with the catchments in the transition zone between the thin and thick till blanket areas. The valley cross-sections are used to compute the volume of material removed as described in Mather et al. (2002) for each basin. The elevations associated with the drainage divides were used to construct a paleosurface of the NMB following a similar method to that described by Brocklehurst and Whipple (2002) and Montgomery and Lopez-Blanco (2003). The lidar DEM was then subtracted from this surface in order to quantify the volume of material removed by glacial-fluvial processes and the patterns of erosion for each basin (Fig. 12).

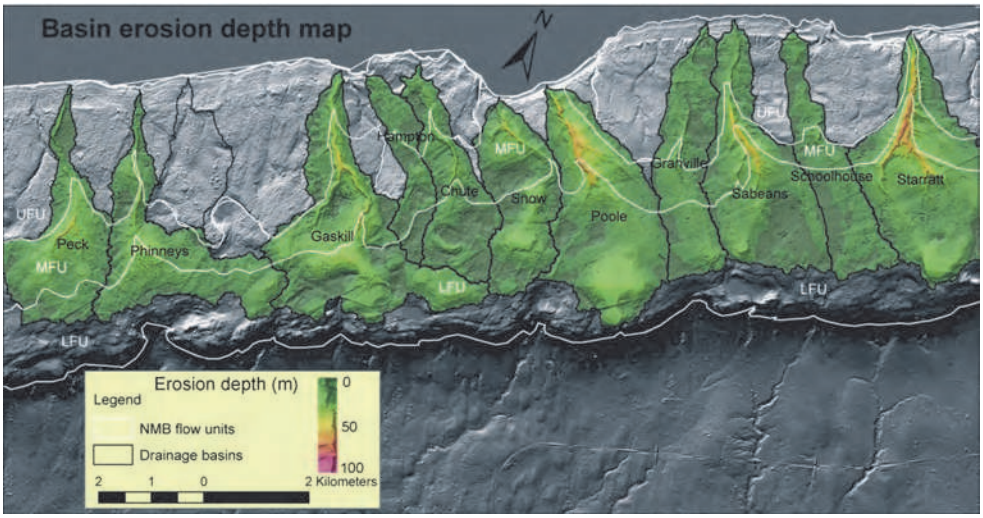

Fig. 12. North Mountain drainage basin erosion depth map with basalt flow unit boundaries. The western basins have incision depth maximums of approximately 50 m and the central and eastern basins have maximum incision depths approaching 100 m.

Erosion rates are calculated from the stream incision depth curves and sediment flux from the erosion depth map assuming erosion began after deglaciation at 12 ka ± 200 yr (1σ) (Stea and Mott, 1998), Table 1.

5. Examples of other lidar DEM geoscience applications

The improved resolution and accuracy under the forest canopy often reveals details that allow traditional geology maps to be improved and contacts between units better defined. Previously, geologists had to rely on sparse outcrop locations along the coast and along

Catchment	Till cover	Volume of sediment removed km³	Maximum sediment flux (km³/ka) assuming erosion started at 12 ka.
Peck	Thin veneer	38.3	3.2
Phinney	Thin veneer	37.4	3.1
Gaskill	Transition zone	81.8	6.8
Poole	Transition zone	91.7	7.6
Sabeans	Thick blanket	47.3	3.9
Starratt	Thick blanket	98.3	8.2

Table 1. Catchments grouped by the amount of till cover and sediment volume removed. Maximum sediment flux per catchment.

stream beds in combination with interpreting aerial photographs that did not penetrate the vegetation canopy. A lidar survey was flown to examine Piping Plover habitat, an endangered shore bird, along the south shore of Nova Scotia (Fig. 13). The area is completely forest covered except along the coast and had been mapped by the Geological Survey of Canada, Open File 1768 (Hope et al., 1988) (Fig. 13).

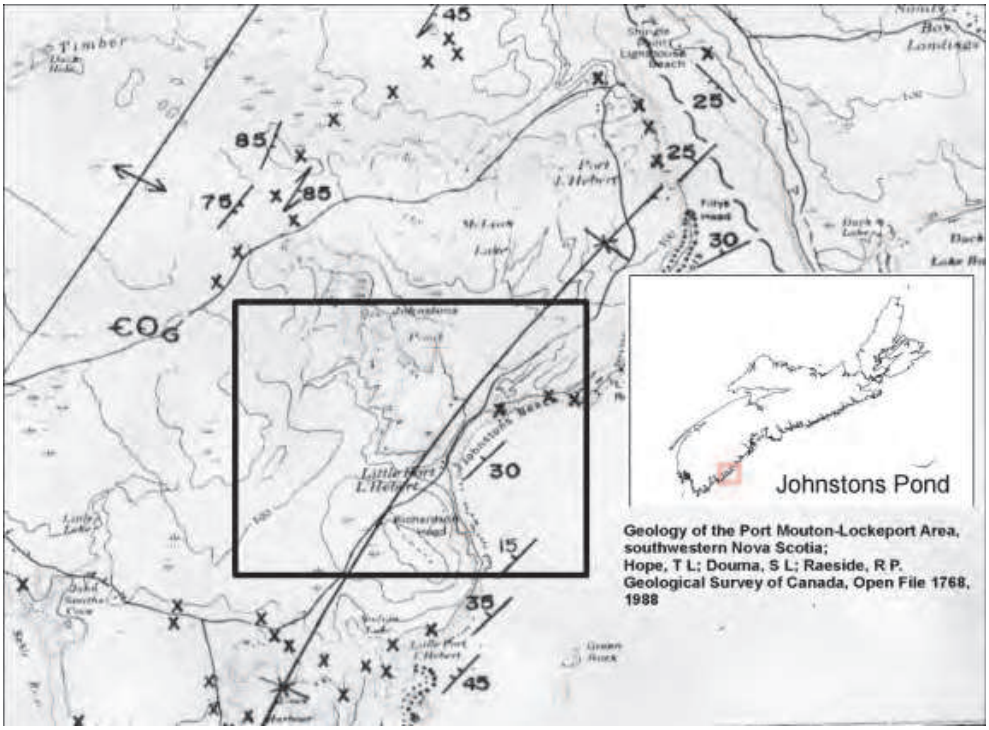

Fig. 13. Geological map of Johnston's Pond area. The black box outlines where the lidar survey was conducted. Note the only geological unit mapped is COg, indicating the Cambro-Ordivician Goldenville formation which is comprised of slates and greywacke. A syncline fold axis passes through the study area.

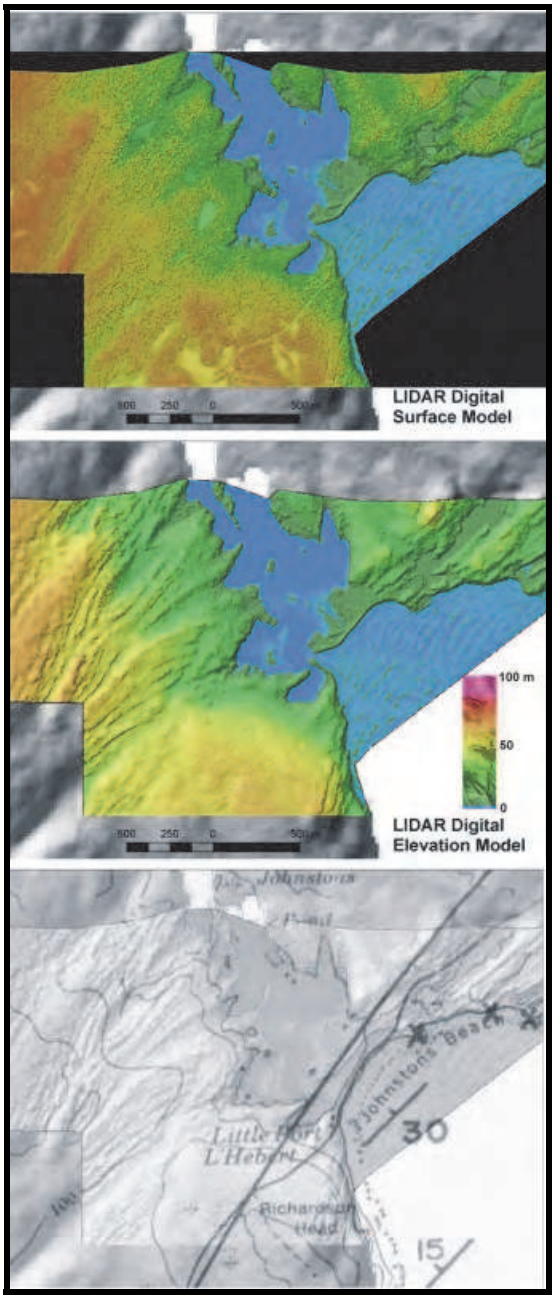

Fig. 14. Lidar surface models. Top: Colour shaded relief of the DSM; Middle: Colour shaded relief of the DEM; Bottom: grey-scale shaded relief of the DEM with the scanned geology (1988).

The lidar survey was conducted during full 'leaf-on' conditions, thus making penetration of the laser pulse to the ground more difficult. The lidar points were classified and surface models constructed, the DSM incorporating all of the lidar returns and the DEM utilizing only the ground points. Colour shaded relief maps of the surface models were constructed and interpreted (Fig. 14). The ability to remove the vegetation points reveals the bedding of the slates and a massive dome structure in the south (Fig. 14). The previous geology indicates that the entire area is made up of sedimentary rocks and is folded into a single syncline which passes directly through the dome structure (Fig. 14, bottom). Based on the visual interpretation of the terrain models, shaded relief and CSR, and a visit to the site for follow up field checks, a new geology map has been derived (Fig. 15). In addition to a new fault being mapped, a granite pluton has also been added to the map. Field evidence to support the occurrence of a fault at this location, where the bedding has been truncated on the CSR DEM, is based on the flat lying sedimentary rocks being tipped vertical in the area proximal to the fault (Fig. 15). A large granite boulder or possible outcrop was found in the field which further supports the interpretation that the topographic dome evident on the lidar is a granite pluton. The variable bed resistance to erosion allows the bedding planes to be traced over large distances even under the forest canopy in the lidar DEM.

Other examples of were the ability to penetrate the forest canopy has assisted geologist in identifying geohazards including sink holes and karst topography is presented next. The Windsor Group represents evaporates, gypsum and salt deposits of Carboniferous age in Nova Scotia. These deposits occur throughout Maritime Canada as sedimentary basins formed on the flanks of the highlands. The area of Oxford, Nova Scotia is used to demonstrate the ability of lidar to map karst topography (Fig. 16). This type of landscape can be a hazard as the bedrock is dissolved by the groundwater and the area can become undermined and local subsidence can occur. The lidar was processed to a DSM and DEM and colour shaded relief maps were constructed (Fig. 16). The bedrock geological boundaries are overlaid to highlight where the Windsor Formation occurs and contain rocks susceptible to the development of karst topography. As can be seen in figure 16, the karst topography crosses under the divided 100 series highway south of the town of Oxford and trends northeast-southwest.

In glaciated terrain, the topography reflects the glacial and fluvial deposits and often masks the bedrock structures. In these areas, the lidar surface models can be used to interpret the unconsolidated sediment deposits and better reconstruct the recent history of the area. If adequate control exists on the locations of bedrock, through outcrop locations or boreholes, a bedrock surface can be constructed and used to derive sediment thickness using the lidar surface model. Lidar was flown along a section of the North Mountain in May 2003 during 'leaf-off' conditions. As mentioned earlier, the North Mountain is underlain by basalt dipping northwest at 6 degrees. Webster et al. (2006) used field checks and the lidar to constrain the individual flow units, especially in areas covered by glacial till. In areas of thick glacial till, the morphology of the flow units is not evident in the lidar because of the smoothed till cover. In this case, planes representing the flow unit boundaries were projected through the DEM and used to define where the flow unit contacts intersected the surface topography (Fig. 17). A series of glacial deposits occur south of Port George along the North Mountain. As a result of the glacial till, the area supports local farms and the land cover is mixed between cleared and forest. The lidar DEM clearly highlights the mound of sediment on the North Mountain (Fig. 18 right). The glacial features evident on the CSR DEM represent a kame deposit with eskers to the south. The kame is formed by the glacier

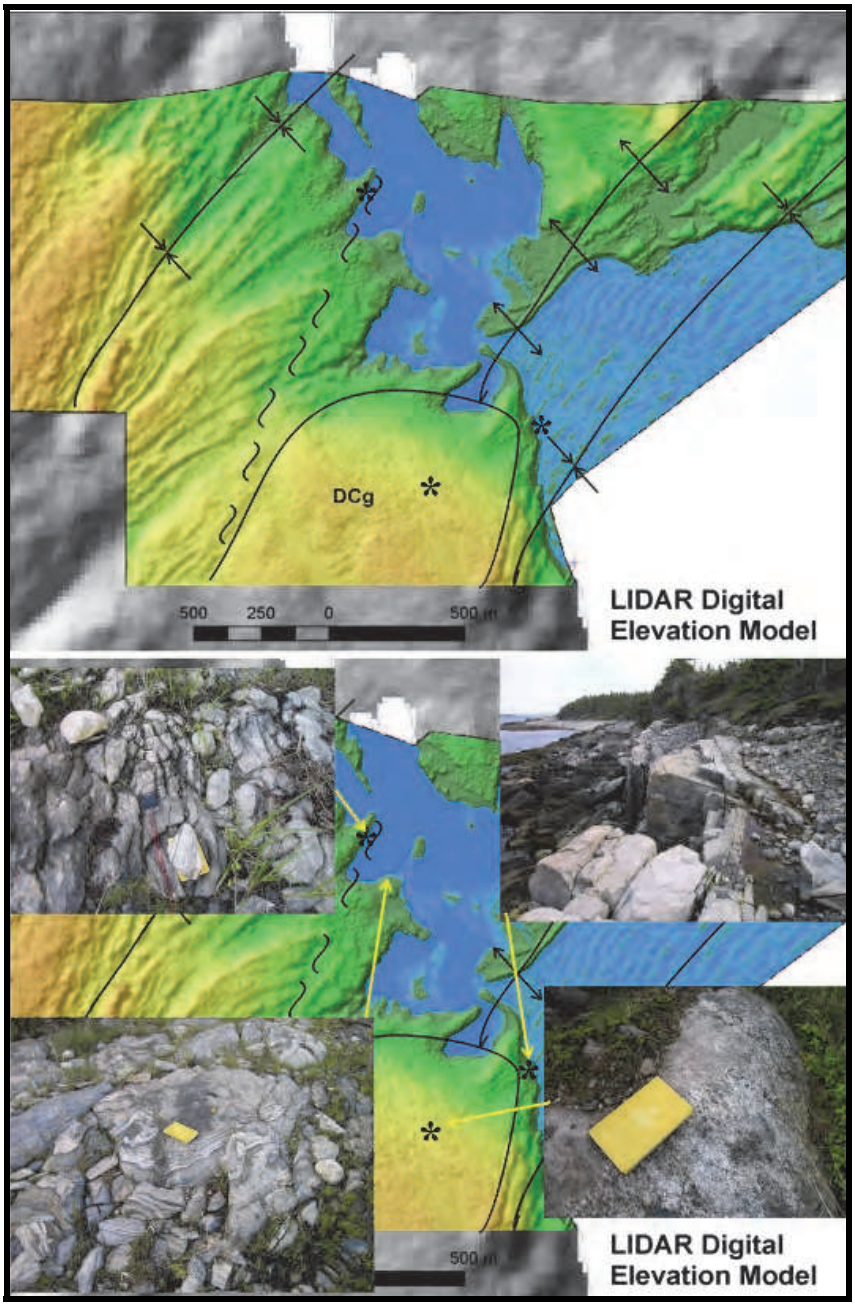

Fig. 15. Top: new interpretation of fold structures and contact between the Goldenville Formation (sedimentary rocks) and granite (DCg large dome to south). Bottom: field photos of rock outcrops that support the interpretation.

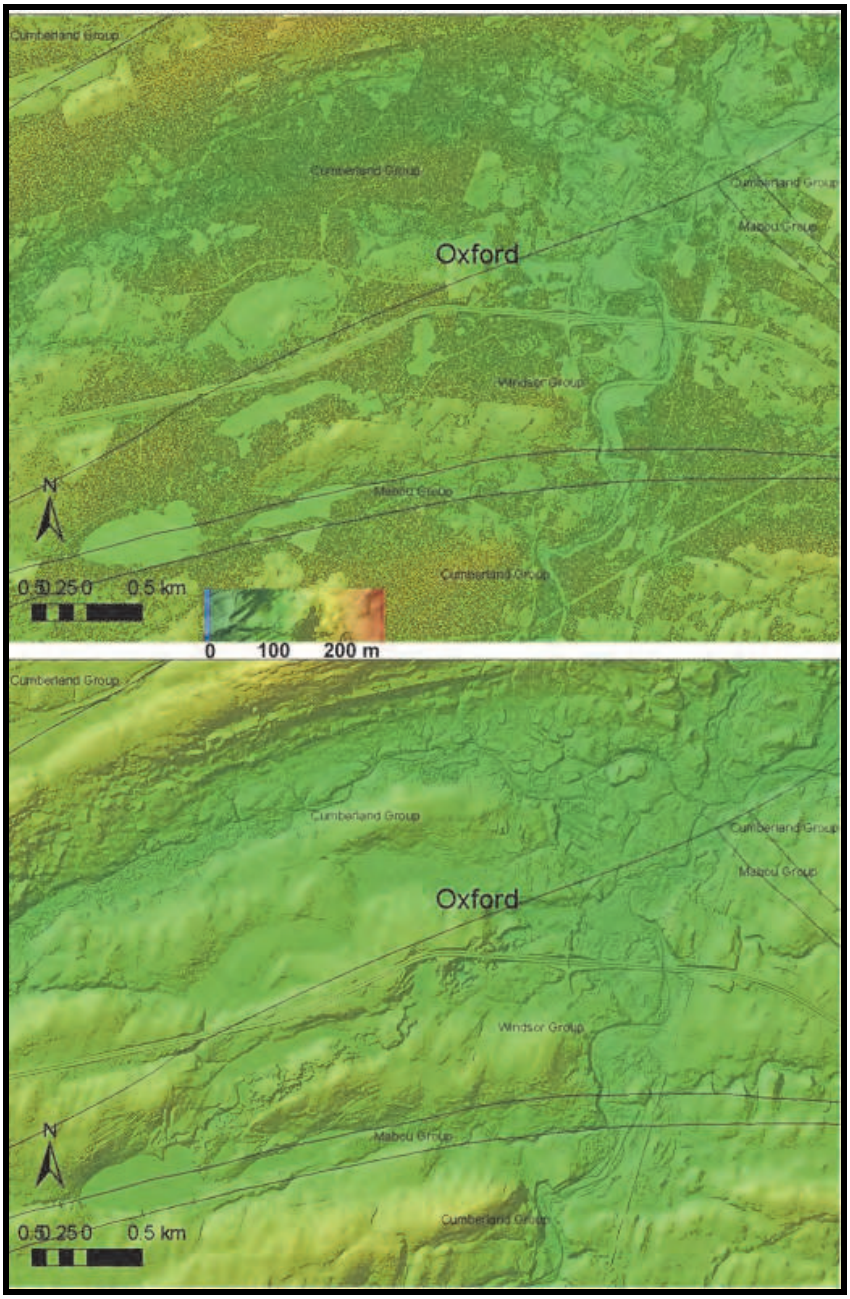

Fig. 16. Top Lidar DSM CSR of Oxford with geological boundaries. Bottom: Lidar DEM CSR with sink holes and karst topography developed below the town of Oxford. Geological boundaries (Keppie, 2000).

remaining stagnant and the trapped sediment dropping out of the ice. The mounds generally do not have well sorted sediment and show no fluvial bedding features. The eskers are the linear ridges running south of the kame and are formed by sediment collected in streams draining the melt-water within the glacier (Fig. 18). The kame and esker systems are comprised more of sand and gravel than the more clay rich glacial till and are a potential aggregate resource.

It appears that the kame and esker deposits are sitting on the bedrock surface or on a very thin glacial till veneer. GIS was used to calculate a surface representing the bedrock, which is dipping at 6 degree northwest (Fig. 19). This surface was constructed by placing a series of points around the perimeter of the kame and esker system and extracting the bedrock elevations from the lidar DEM. The points were then used to construct a TIN and a raster surface was extracted from the TIN using a linear interpolation method (Fig. 19).

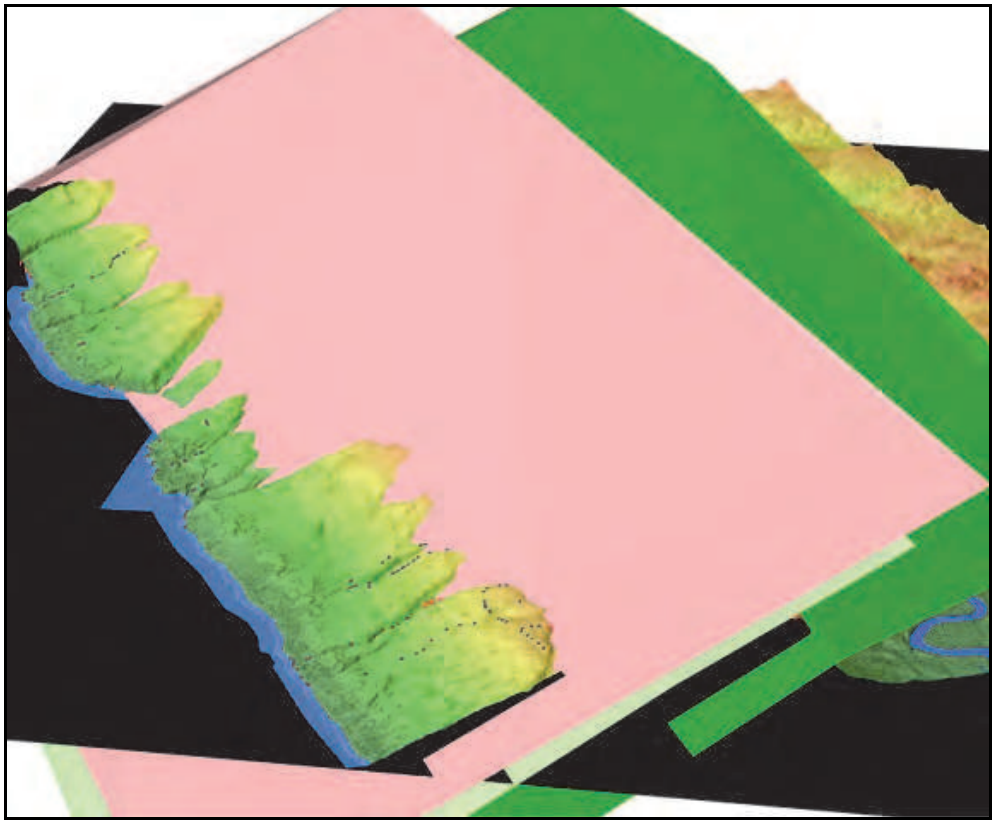

Fig. 17. Basalt flow unit contact planes projected through the lidar DEM. The pink plane represents the contact between the Upper Flow Unit (UFU) and the Middle Flow Unit (MFU), the light green plane represents the boundary between the MFU and lower Flow Unit (LFU) and the dark green plane represents the base of the LFU. Adapted from Webster et al. 2006.

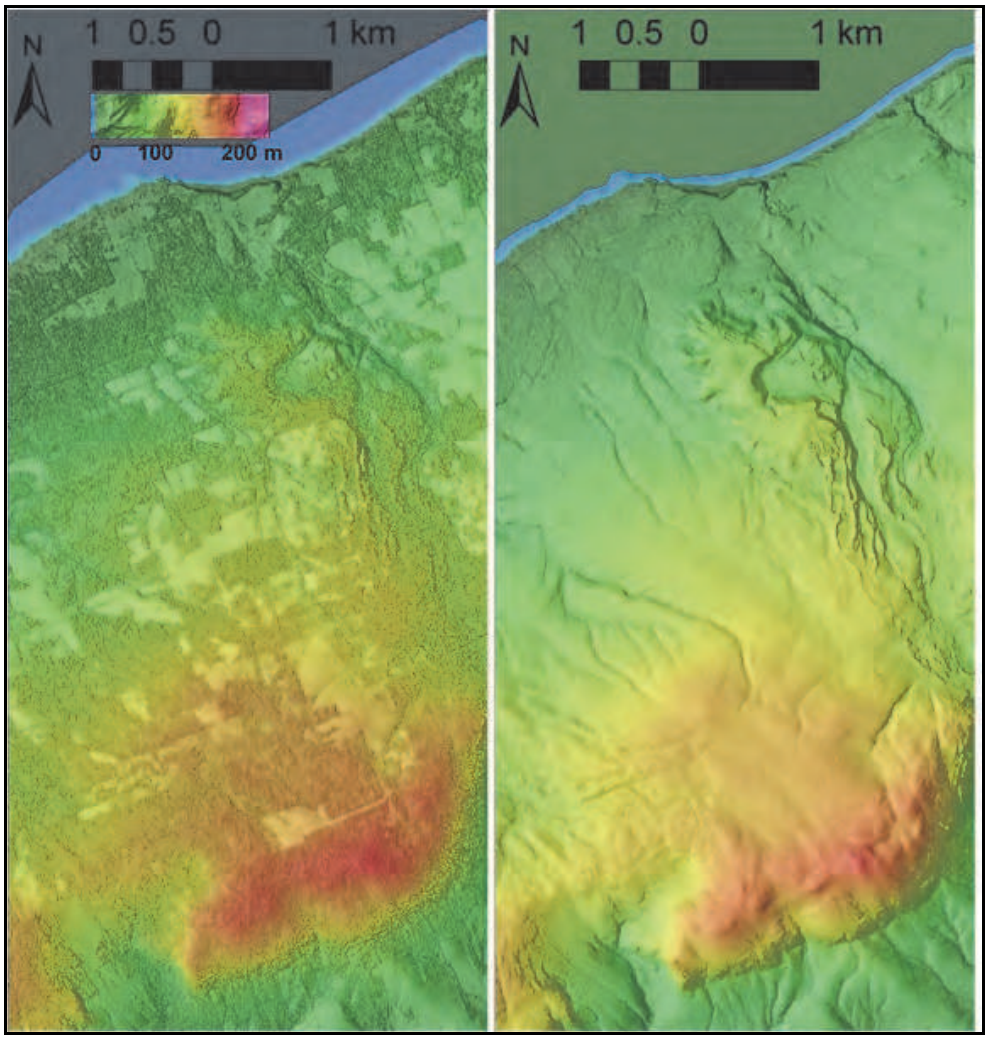

Fig. 18. Port George colour shaded relief lidar surface models. Left: DSM; Right: DEM with the kame and esker glacial deposits clearly visible.

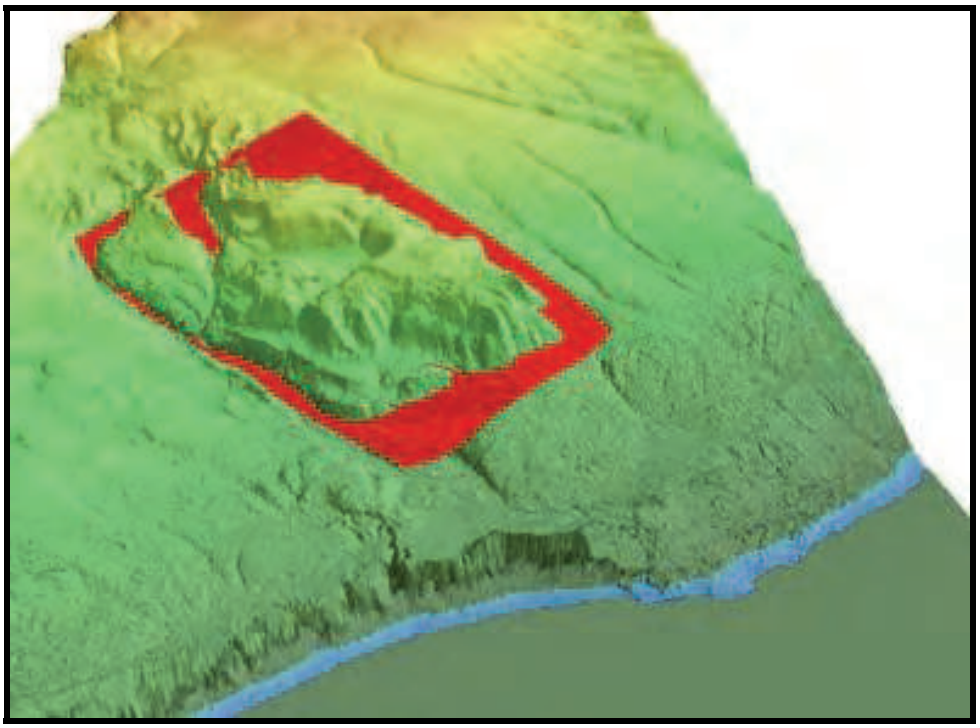

Fig. 19. Perspective view of the lidar DEM along the North Mountain. The red plane represents the bedrock surface that intersects the DEM.

This new surface was used to calculate the thickness of the kame deposit by subtracting the lidar DEM from the bedrock planar surface (Fig. 20). Once the sediment thickness is calculate the volume of sediment can be easily derived. This allows the landowner to assess the potential value of the aggregate resource. As can be seen in figure 20 the thickness is up to 60 m in places and represents a significant amount of material that is available as an aggregate resource.

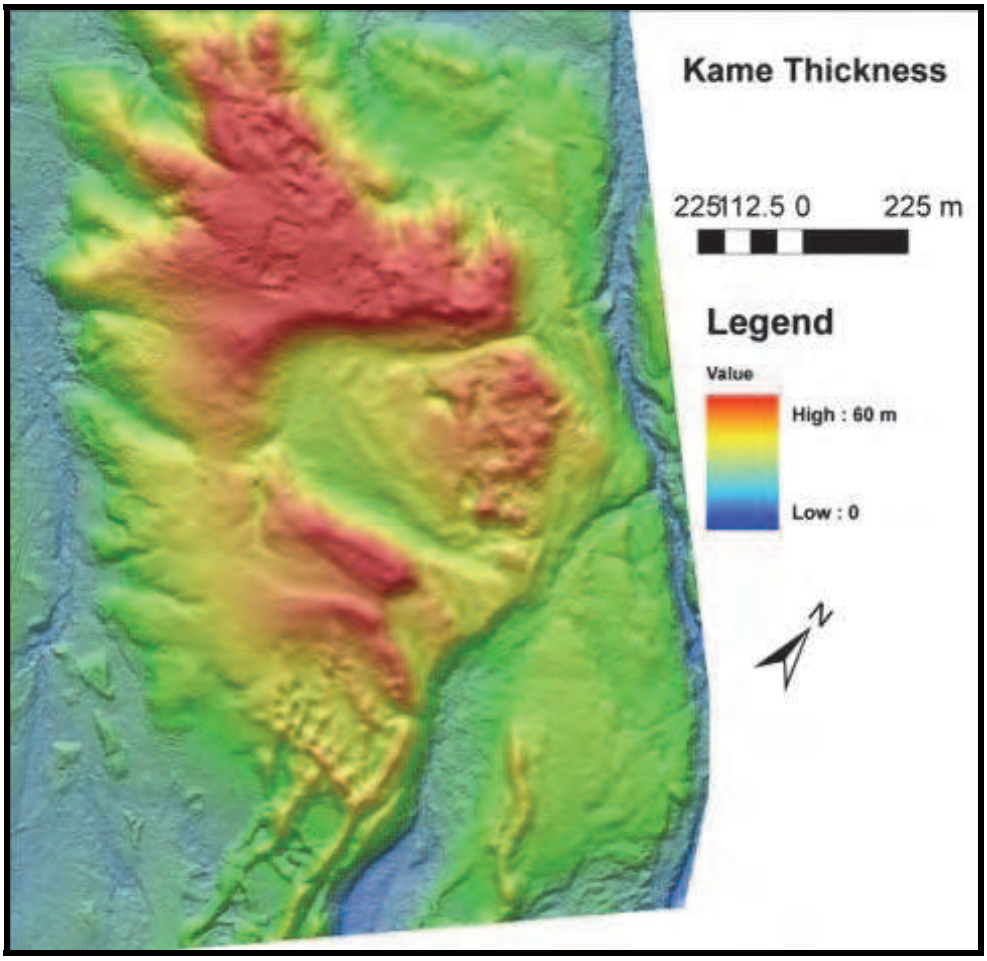

Fig. 20. Thickness of the sediment associated with the kame deposit along the North Mountain near Port George, Nova Scotia.

In some locations along the North Mountain the glacial deposits are thicker than others where ice moved into the Bay of Fundy. In areas of thicker glacial deposits along the coast, the raised beach terraces are more pronounced in the lidar DEM (Webster et al., 2006, A). These terraces represent sea-levels that where 35 m higher than present ca. 12,000 years ago. These higher sea-levels occurred after deglaciation when the melt-water caused the ocean to rise faster than the crust rebounded forming these terraces at the highest elevation.
As noted earlier the influence of glacial till over parts of the North Mountain have smoothed the topography which contrasts between the rough terrain where there is a thin veneer of glacial till and the basalt flows are evident and the smoothed surfaces where the glacial till is thickest (Figs. 6-8). Topography can exhibit a sense of being fractal, which means the measurements we make of the terrain surface are a function of the scale at which we make the measurements (Turcotte, 1992). In other words, the terrain will appear rougher and

more undulating as you make observations at larger and larger scales (more detail and smaller areas), as compared to measurements of the terrain taken from data at smaller and smaller scales or courser resolution. Fractal roughness is the difference between the terrain undulations as measured from data at two different scales. To attempt to quantify the difference in roughness between the thin and thick glacial till areas along the North Mountain, a method has been devised that approaches a measure of fractal roughness (Fig. 21).

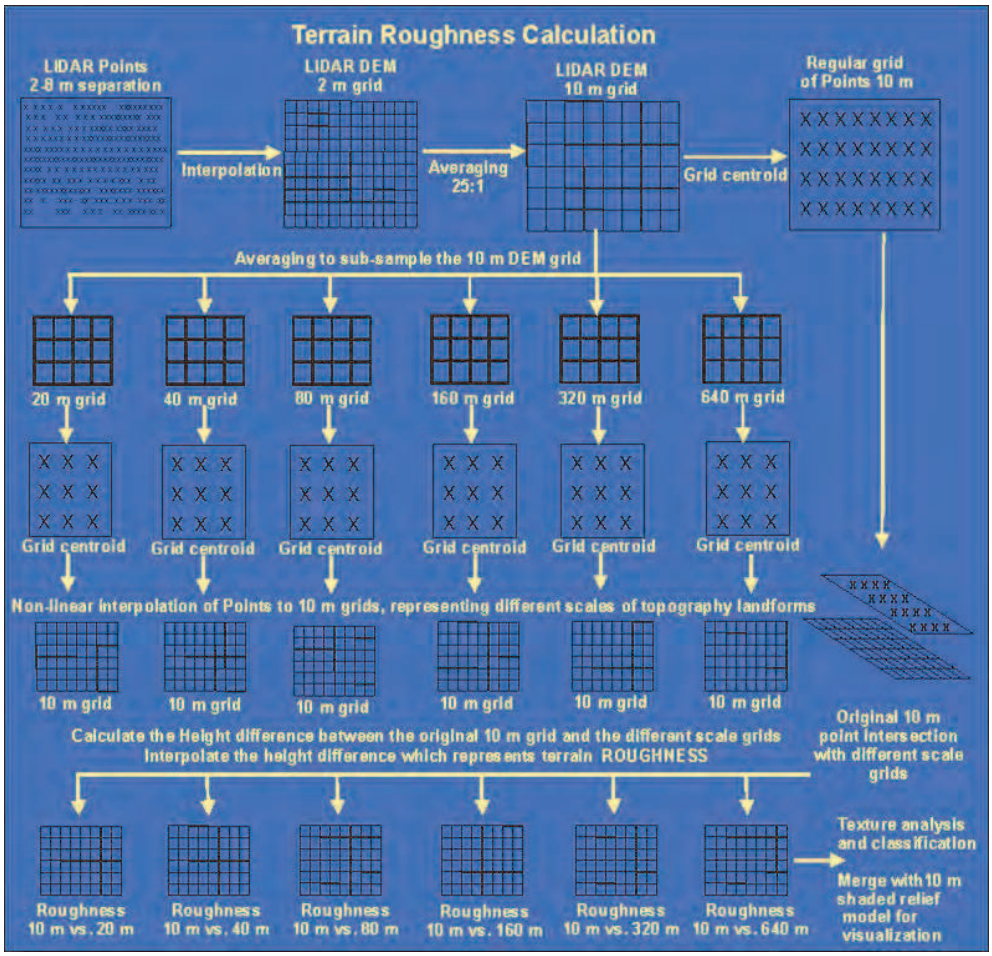

Fig. 21. Schematic of the data processing algorithm to calculate terrain roughness at different scales. Grids are represented by the square grid pattern and points are represented by "X" patterns.

The method involves starting with the irregular point spacing of the classified lidar 'ground' points and interpolating a DEM surface to a regular grid cell size of 2 m. This DEM grid is then averaged to a 10 m grid cell to facilitate processing and reduce the degree of noise of the surface. The 10 m grid is then converted back to points based on the grid centroid

locations and assigned the elevation of that cell. The 10 m grid is also sampled up in resolution using an averaging technique to coarser and course DEMs of 20, 40, 80, 160, 320 and 640 m respectively. The choice of what grid cell resolution to resample to is dependent on the scale of the terrain features of interest. In this case, the grid cell resolution was increased by a factor of two each time for the purpose of demonstrating the technique (Fig. 21). These averaged DEMs of variable resolution are then converted to point centroids, where the point spacing would equal the grid cell spacing. These points are then non-linearly interpolated to 10 m grids, where each represents a different scale (decreasing scale with increasing point-grid cell spacing) of the terrain. The original 10 m grid cell points are then used to extract the elevation values from the variable scale grids and the difference between the 10 m scale elevation and the variable scale elevation is calculated. This difference in elevation, from different scale representations of the terrain, is then used to interpolate a new grid which represents the roughness or difference in roughness between the 10 m scale and the coarse scale grids (Fig. 21). The roughness grids have positive and negative values representing valleys and hills respectively on the 10 m DEM that are smoothed over as one moves to coarser and coarser scales of the topography. Profiles were extracted from the different roughness grids for a section of the North Mountain where the glacial till is thin and where it is thick (Fig. 22). The actual roughness profiles for the two

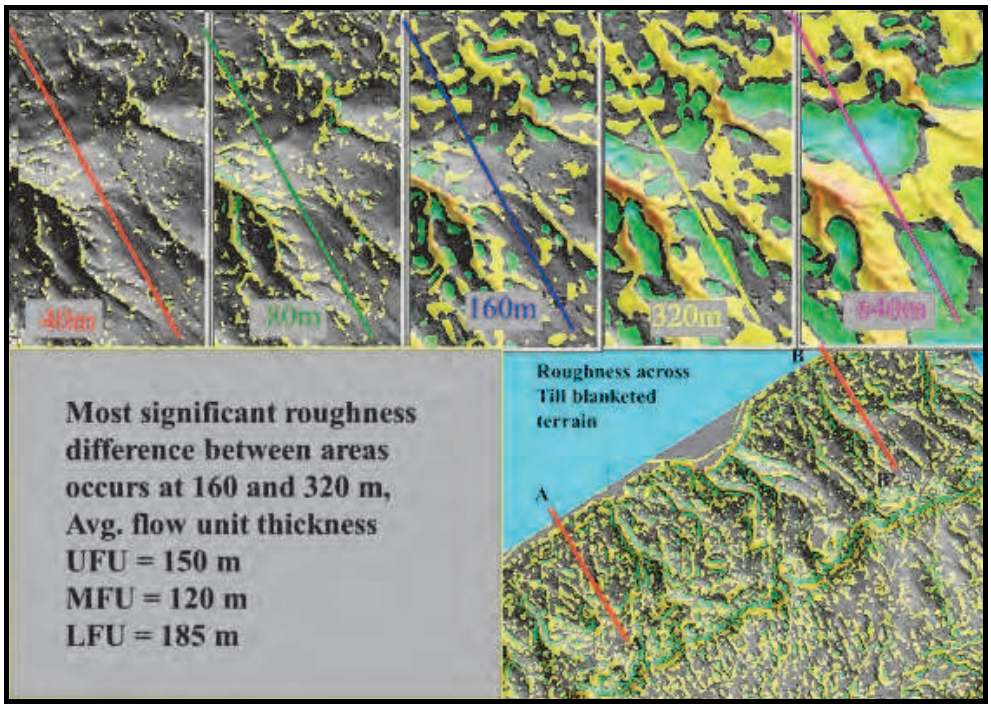

Fig. 22. Example of different terrain roughness grids along the North Mountain. Profile location A-A' is in the area of thin till and rough terrain, while profile B-B' is in the area of thick till and smoother terrain (See Fig. 23 for profiles). The top series of maps shows the location of profile B-B'.

locations are presented in figure 23. As can been seen in this figure the magnitude of the roughness difference between the two sites is significant with profile B-B′ being smoother. The differences in roughness at scales of topography closer to the 10 m grid show less differences between the two areas (e.g. 40 and 80 m grid differences) (Fig. 23). The most significant differences between the two profiles occurs once the scale of the DEMs are above 160 m (Blue line Fig. 23). This scale is interpreted to be related to the average volcanic flow unit thicknesses which varies between 150-185 m and are the dominant features that are causing the roughness in the areas of thin glacial till.

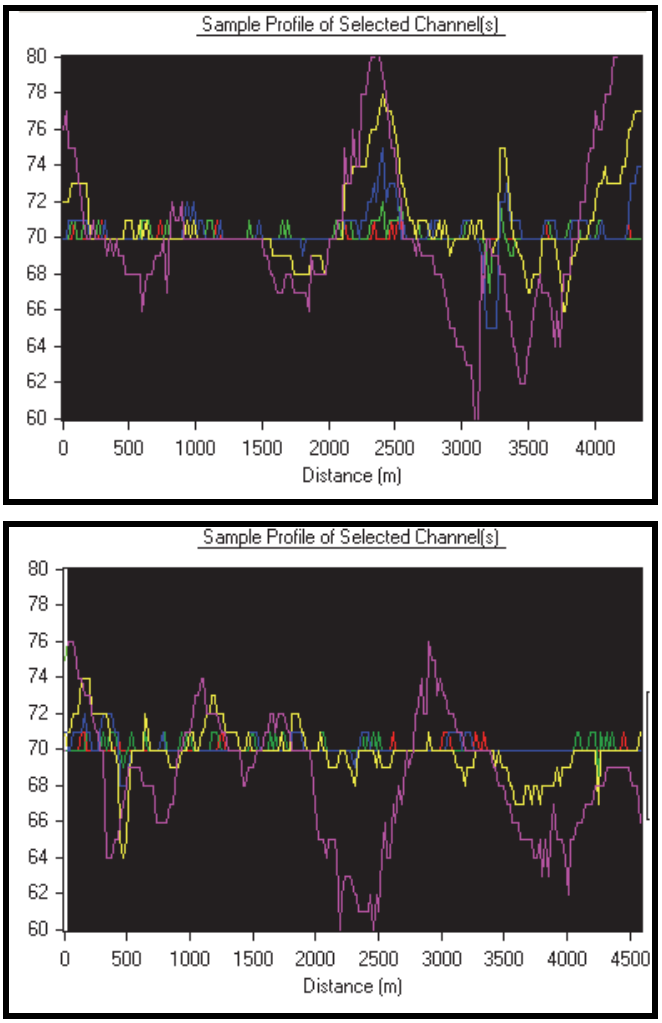

Fig. 23. Profiles of terrain roughness. Top graph is for profile A-A' in Fig. 22 thin glacial till, Top graph is for profile B B' in Fig. 22 thick glacial till. The colour of the profile line corresponds to the line and colour used for the different scales of topography (ie. 40 - red, 80 - green, 160 – blue, 320 - yellow and 640 m – magenta respectively Fig. 22).

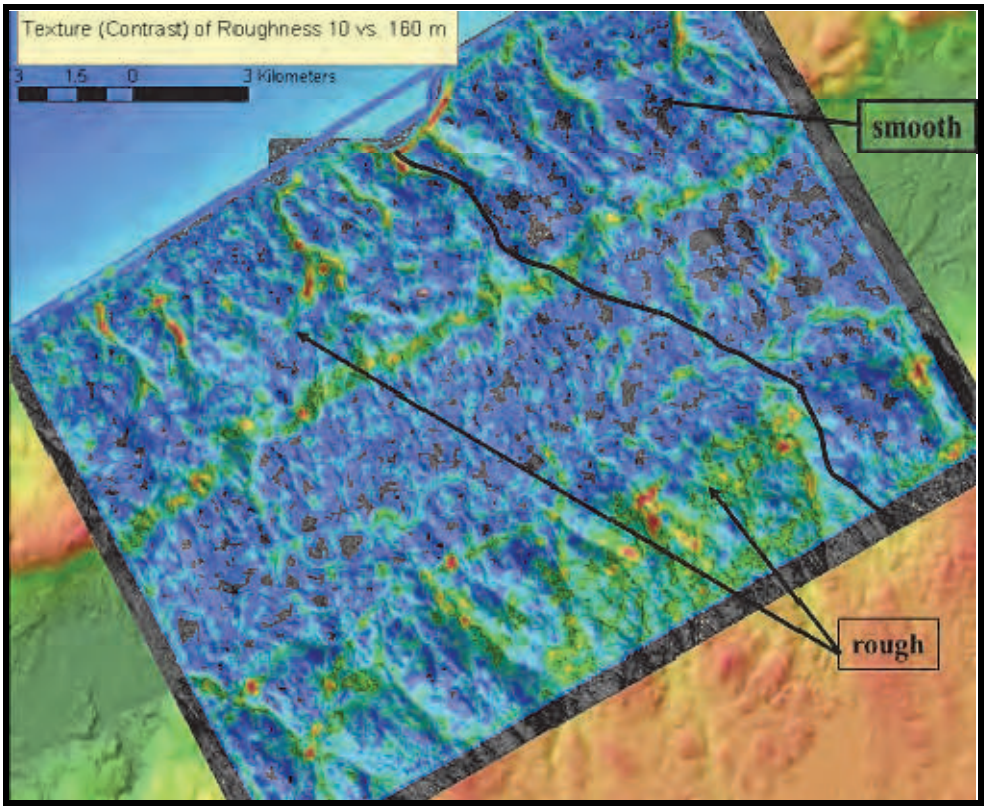

Fig. 24. Texture measure of the roughness grid derived from the difference of the 160 m grid cell terrain and the 10 m grid cell terrain map. Note the patches of dark grey represent a low texture value, or low roughness. The grey boarder around the map is no data.

A further metric was calculated from these difference roughness grids in the form of a texture measurement, which is typically related to the variance or standard deviation of the grid cell values within a moving window. The difference in roughness between the two profile locations begins to be significant at the 160 m scale; this roughness grid was used to calculate the texture in order to determine if the terrain is quantifiably different in these locations (Fig. 24). This map shows a significant contrast between the thick and thin glacial till cover, as marked by the heavy black line across the map. This difference in texture is more pronounced when applied to the 160 m scale roughness map than any of the original lidar DEMs at variable scales.

This approach of quantifying the degree of roughness of the terrain may help in eventually forming a fully automated landscape classification system. For example, if we examine the roughness difference grid at the 320 m scale, we can identify the streamlined landforms and drumlins within the valley floor (Fig. 25). The green areas represent topographic highs and the yellow areas represent topographic lows and the grey background represents smooth terrain (Fig. 25). This approach produces results that can complement other methods where the degree of curvature is estimated for the terrain, ie. concave or convex slopes, which are

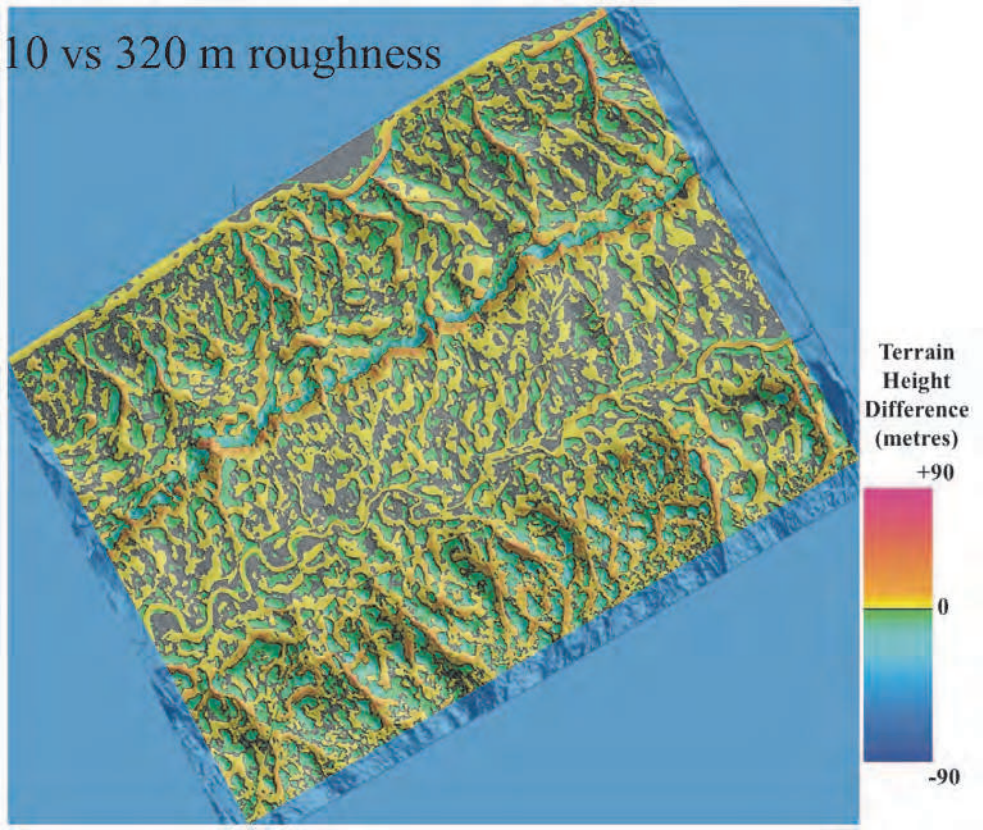

Fig. 25. Example of roughness grid difference between topographic scale 320 m and 10 m. Note the drumlins and streamline glacial landforms are highlighted in the valley floor as well as some of the basalt flow unit boundaries on the North Mountain.

calculated using the second derivative of the DEM. This method can be tailored to the scale of the topographic features of interest and through GIS processing, the features can be automatically extracted and quantified.

Recent advances in laser mapping technology have developed "mobile mapping" systems where laser scanners have been deployed on land and marine vehicles instead of aircraft. One disadvantage of an airborne lidar system is that it does not sample or measure the terrain of steep slopes very well and certainly not of any areas that are covered by an overhang because of the viewing geometry of the system. As a result of this limitation of airborne systems, steeper slopes and cliffs along the coast are not well resolved with airborne lidar DEMs. As with urban buildings and other structures, the cliff face is not resolved to the same level of detail as the rest of the terrain. This limitation affects the ability of airborne lidar to be used for detailed coastal change in these environments. In this case a laser scanner can be setup on the beach and the coastal cliff section can be imaged to capture all of the detail and merged with the airborne lidar to form a complete 3-D surface of the terrain. In urban landscapes, "mobile mapping" systems are being used to capture the sides

of the buildings and all of the street furniture (e.g. signs, light poles, fire hydrants etc.). Joggins, Nova Scotia is a world UNESCO Heritage site because of the Carboniferous fossils that occur there in the outcrop exposed along the coast. Unfortunately the cliffs are actively eroding and expected to erode faster as sea-levels rise. An airborne lidar survey was conducted over the area in 2007 and a follow up ground-based lidar survey was conducted in 2009 to obtain details on the cliff face and monitor erosion (Fig. 26). Repeat ground-based surveys are planned in order to measure the change along the cliff face.

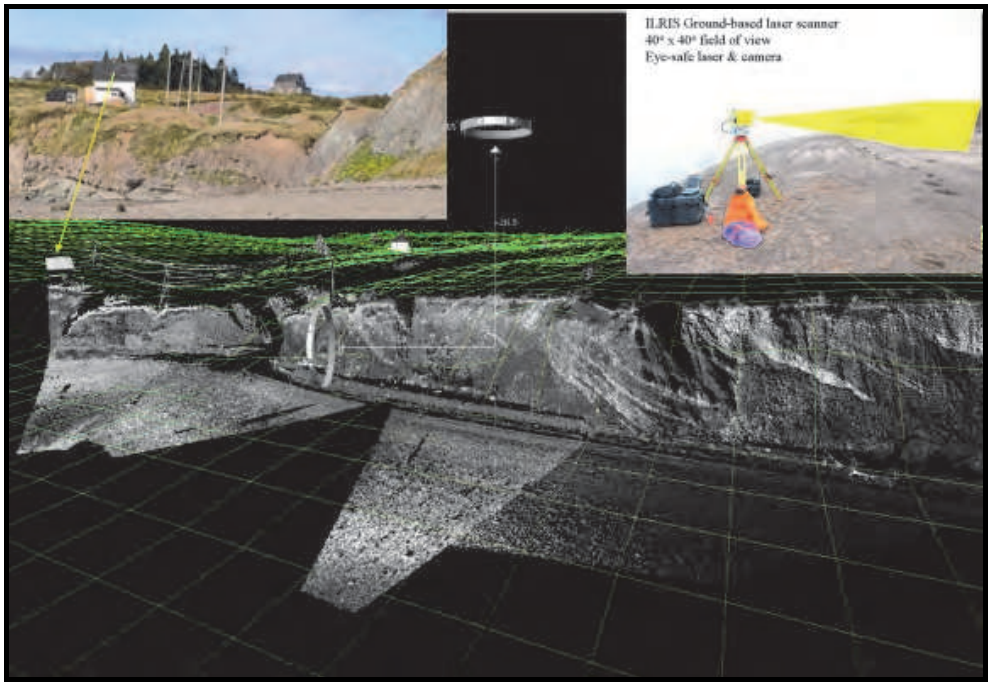

Fig. 26. Point clouds of ground-based lidar scans displayed as grey-scale intensity of the fossil cliffs at Joggins, NS. The wire frame diagram in the background is from an airborne lidar DEM. The top left photo shows the location of a house and power lines at the top of the cliff. The top right photo shows the lidar setup on the beach to image the cliff.

Other coastal areas in Nova Scotia are comprised of glacial till and are even more susceptible to erosion from the sea. Repeat ground-based lidar surveys were conducted at Cape John, Nova Scotia in 2010 and 2011 in order to measure the effects of winter storms on the coastline. Targets are placed within the landscape to be scanned and positioned using survey grade GPS. Once the terrain is scanned, a lidar point cloud can be georeferenced by identifying the targets and their coordinates to transform them into a map projection system so they can be integrated with other spatial data in a GIS. DEMs at 20 cm grid cells representing the bank were constructed from the georeferenced point clouds. Surveys were conducted in Dec. 2010 and Jan. 2011 after a major storm surge event on Dec 21 and 28th 2010 impacted the area. The DEMs from Dec. and Jan. were subtracted to map out the differences in the terrain and calculate the volume of sediment removed during the storm event (Fig. 27). Along a 150 m stretch of the

coast, 771 cubic metres of sediment were removed based on the DEM analysis (Fig. 27). The storm surge associated with this event was 1.5 m above the usual water level and a local tide gauge measured the maximum water level to be 2.21 m above CGVD28 or approximate mean sea-level. This does not include breaking waves or wave run-up. A profile of the DEM before (Dec. 16) and after (Jan. 4) the storm indicates the erosion of the bank reached the 4.75 m elevation level. The erosion profile is typical of a coastal section where the tow of the sloped bank has been removed, causing the bank slope to steepen, and some of the material deposited in the near shore. The bank was frozen at the time of the second survey and could not maintain the steep slope and has since slumped during the spring thaw cycle to a stable slope causing the top of the bank to further retreat from the coast.

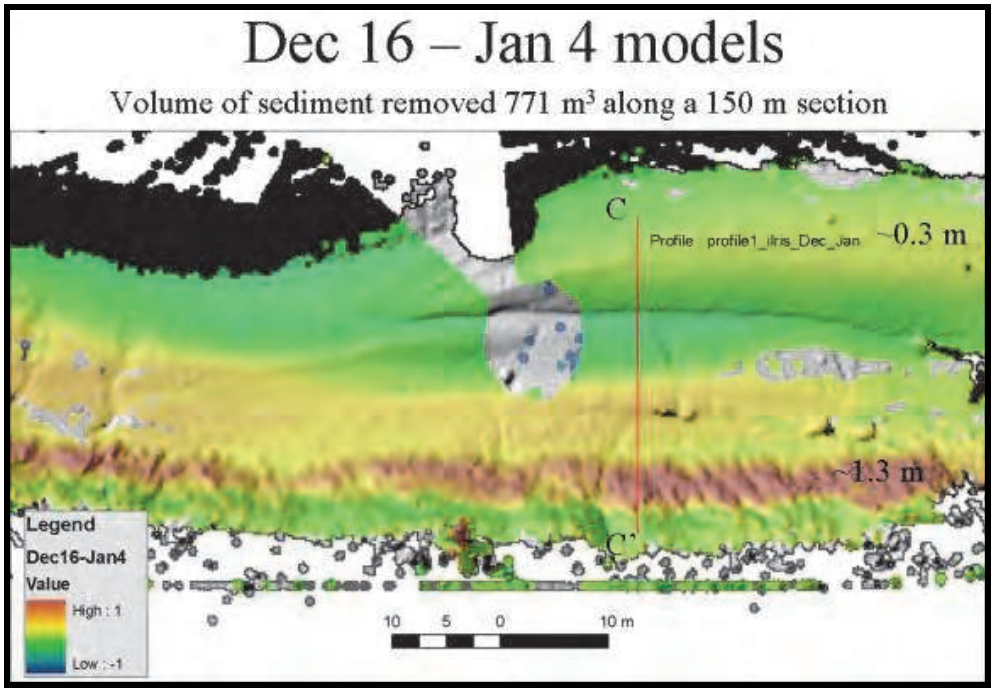

Fig. 27. Difference grid of Dec. and Jan. DEMs derived from ground-based lidar. Note the profile location C-C′.

This approach of utilizing a ground-based lidar allows for detailed analysis of changes of steep slopes that are not easily resolved with airborne techniques. The approach also has the advantage of allowing for quick deployment and is less expensive than an airborne survey. The method is fairly labour intensive and requires targets to be setup and precisely surveyed in order to georeference the scan. The latest "'mobile mapping" systems are equipped with a similar navigation system as the airborne lidars that provide a solution based on the GPS position of the sensor and the angular measurements of an IMU. As a result, the lidar scans are automatically georeferenced in a similar fashion as with the airborne systems, although some urban and cliffed environments present challenges to good GPS satellite reception.

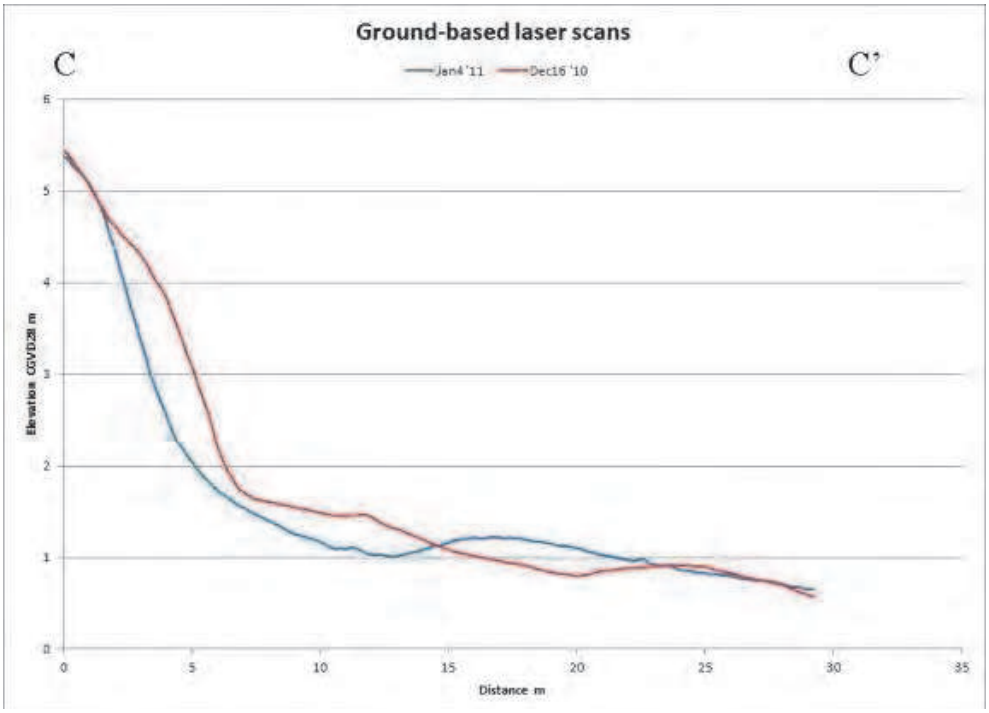

Fig. 28. Profile of coastal glacial till bank at Cape John, NS. before (Dec. 16 - red profile) and after (Jan. 4 – blue profile) a major winter storm event that occurred on Dec. 21, 2010. The upper erosion limit is at the 4.75 m elevation and the bank has been significantly steepened.

6. Conclusions

The objectives of this chapter were be to describe what terrain mapping lidar is and what map products can be derived from it. The ability of lidar to penetrate small openings in the forest canopy and sample the bare earth surface has revolutionized the accuracy and the way DEMs are constructed and used by Geoscientists. This review of lidar included the hardware and software involved in data collection and initial processing at a high level. The lidar point cloud must be processed and the ground points classified. Various surface models can be constructed from the classified point cloud including the Digital Surface Model, incorporating all of the lidar points (ground, buildings and vegetation), and of more importance to the geoscience community the DEM can be constructed by incorporating only the ground points into the model. An additional data product available from a lidar survey is based on the intensity of the reflected lidar pulse. All of the lidar point intensities are used to build the model which essentially resembles a near infrared photograph depending on the wavelength of the lidar laser system, typically 1064 nm. Once the lidar data are processed to map products, various GIS and image processing routines are applied to these data to allow visual and analytical interpretation (shaded relief maps for example).

Since the lidar only provides insights into the surface topography, the concepts of data integration and the generation of hybrid image maps were explained and demonstrated. For example, the grey scale shaded relief lidar was merged with geophysical data in the form of a radiometric survey of equivalent uranium and thorium. Different geophysical datasets can be integrated with the lidar to better understand the relationship between the surface topography and shallow structures and contacts (1st derivative magnetics), to deeper features (e.g. total field magnetics, Bouguer gravity). In glaciated terrains, the topography reflects the surficial deposits of unconsolidated material. The lidar DEM often reveals previously unseen details of the earth's surface that can be used to refine and revise geological maps. This was demonstrated in areas of folded and faulted sedimentary rocks in contact with a granitic pluton. In glaciated terrains, the lidar surface models were used to interpret the glacial and fluvial history of several areas in Nova Scotia. Lidar DEMs were used to measure modern surface processes such as fluvial incision and erosion. GIS and the lidar DEM were used to automatically extract watersheds and longitudinal stream profiles where knick points can be observed and related to erosion rates. Lidar surface models were also used to map geohazards in the form of sink holes and karst topography. In glaciated terrains, the thickness of the unconsolidated material associated with the glacial deposits was calculated using standard GIS techniques. The sediment thickness was calculated by constructing a bedrock surface and subtracting it from the lidar surface model. Other applications of lidar DEMs included research methods to quantify terrain roughness differences in areas of thin glacial till and areas of a thicker till blanket.

Lastly, the chapter concluded with the latest in lidar mapping which includes the use of ground-based scanners and "mobile mapping" which allows the lidar to be mounted on land and marine vehicles. This type of technology can be used to monitor the amount of material removed at open pit mines or gravel quarries. The application of a ground-based lidar was demonstrated to survey a bedrock cliff to establish a baseline of information. Repeat lidar surveys will be used to monitor the rate that the cliff is actively eroding since it is an important fossil heritage site. The impact of storm surge and erosion on a glacial till

bank was demonstrated by comparing repeat ground-based lidar surveys. The volume of sediment eroded during a storm event was quantified and the vertical limit of erosion was measured from the lidar derived DEMs of the bank.
Geomatics offers the geoscientist a wide suite of data, tools and techniques to further our understanding of geology and earth surface processes.

7. Acknowledgements

There are several people who have contributed to the research presented in this chapter that I would like to thank. The lidar for the North Mountain was acquired with a grant from the Canada Foundation for Innovation. Some of the research related to the North Mountain was part of my PhD research that was funded through the NSCC and Brendan Murphy of St. Francis Xavier University. Also I would like to acknowledge my PhD supervisors: John Gosse of Dalhousie University, Ian Spooner of Acadia University and Brendan Murphy of St. Francis Xavier University. Lidar for the Oxford and Johnstons Pond areas was flown by AGRG and I would like to thank Bob Maher, Chris Hopkinson, Allyson Fox, David Colville, Ryan Goodale and Doug Stiff for their involvement in those projects. Other research interns and partners who contributed include Angela Templin, and Gordon Dickie and Matt Ferguson of Shaw Resources. The coastal fieldwork team for the repeat surveys of Cape John included Nathan Crowell, Kevin McGuigan and Candace MacDonald. Thanks to Grant Wach and Christian Rafuse for the use of Dalhousie Universities ILRIS laser scanner for the Dec. and Jan. surveys at Cape John. Funding for the repeat surveyes was provided by Will Green of the NS Department of Environment. The Joggins ground surveys were conducted with assistance from Nathan Crowell, Stephanie Rogers, Danik Bourdeau, and Kate Leblanc.

8. References

Belt, K. and Paxton, S.T. 2005. GIS as an aid to visualizing and mapping geology and rock properties in regions of subtle topography. Geological Society of America Bulletin, 117, no. ½: 149-160.

Brock, J.C., Wright, C.W., Sallenger, A.H., Krabill, W.B., Swift, R.N. 2002. Basis and methods of NASA airborne topographic mapper LIDAR surveys for coastal studies. Journal of Coastal Research, 18: 1-13.

Brocklehurst, S.H. and Whipple, K.X. 2004. Hypsometry of Glaciated Landscapes. Earth Surface Processes and Landforms, 29: 907-926.

Costa-Cabral, M.C. and Burges, S.J. 1994. Digital Elevation Model Networks (DEMON): A model of flow over hill slopes for computation of contributing and dispersal areas. Water Resource Research, 30, no. 6: 1681-1692.

Charlton, M.E., Large, A.R., and Fuller, I.C. 2003. Application of airborne LIDAR in River Environments: The River Coquet, Northumberland, UK. Earth Surface Processes and Landforms, 28: 299-306.

ChromaDepth 3-D Glasses. www.Chromatek.com

Dietrich, W.E., Bellugi, D.G., Sklar, L.S., Stock, J.D., Heimsath, A.M., and Roering, J.J. 2003. Geomorphic Transport Laws for Predicting Landscape Form and Dynamics. *In* Prediction in Geomorphology. Geophysical Monograph 135, pp. 1-30.

Dostal, J., and Dupuy, C. 1984. Geochemistry of the North Mountain Basalts (Nova Scotia, Canada). Chemical Geology, 45: 245-261.

Flood, M. and Gutelius, B. 1997. Commercial implications of Topographic Terrain Mapping Using Scanning Airborne Laser Radar. Photogrammetric Engineering and Remote Sensing, 4: 327-366.

Gomes Pereira, L.M. and Wicherson, R. J. 1999. Suitability of laser data for deriving geographic information - a case study in the context of management of fluvial zones. International Journal of Photogrammetry and Remote Sensing, 54, no. 2-3: 105-114.

Harding, D.L., and Berghoff, G.S. 2000. Fault scarp detection beneath dense vegetation cover: Airborne lidar mapping of the Seatle fault zone, Bainbridge Island, Washington State. *In* Proceedings of the American Society of Photogrammetry and Remote Sensing Annual Conference, Washington, D.C., pp. 9.

Haugerud, R.A., Harding, D.J., Johnson, S.Y., Harless, J.L., Weaver, C.S., and Sherrod, B.L. 2003. High-resolution lidar topography of the Puget Lowland-A bonanza for earth science. Geological Society of America Today, 13, no. 6: 4-10.

Hope , T.L., Douma, S.L., Raeside, R.P. 1988. Geology of Port Mouton-Lockeport Area, southwestern Nova Scotia. Geological Survey of Canada Open File 1768.

Jenson, S.K., and Dominque, J.O. 1988. Extracting Topographic Structure from Digital Elevation Data for Geographic Information Systems Analysis. Photogrammetric Engineering and Remote Sensing, 54, no. 11: 1593-1600.

Kirby, E. and Whipple, K. 2001. Quantifying differential rock-uplift rates via stream profile analysis. Geology, 29, no. 5: 415-418.

Kooi, H. and Beaumont, C. 1996. Large-scale geomorphologt: classical concepts reconciled and integrated with contemporary ideas via a surface-process model. Journal of Geophysical Research, 101: 3361-3386.

Krabill, W.B., Thomas, R.H., Martin, C.F., Swift, R.N., and Frederick, E.B. 1995. Accuracy of airborne laser altimetry over the Greenland ice sheet. International Journal of Remote Sensing, 16: 1211-1222.

Krabill, W., Abdalati, W., Frederick, E., Manizade, S., Martin, C., Sonntag, J., Swift, R., Thomas, R., Wright, W., and Yungel, J. 2000. Greenland Ice Sheet: high-elevation balance and peripheral thinning, Science 289: 428-430.

MacDonald, M. A. and Ham, J.A. 1994. Geological Map of Bridgetown, South Mountain Batholith Project. Nova Scotia Department of Natural Resources, Halifax N.S. Map 94-08.

Mather, A.E., Stokes, M., and Griffiths, J.S. 2002. Quaternary Landscape Evolution: A Framework for understanding contemporary erosion, southeast Spain. Land Degradation & Development, 13: 89-109.

Maune, D. F. 2001. Digital Elevation Model Technologies and Applications: The DEM Users Manual. *Edited by* D.F. Maune, American Society of Photogrammetry and Remote Sensing. pp. 1-250.

McKean, J., and Roering, J. 2003. Objective landslide detection and surface morphology mapping using high-resolution airborne laser altimetry. Geomorphology, 1412: 1-21.

Montgomery, D.R., and Lopez-Blanco, J. 2003. Post-Oligocene river incision, southern Sierra Madre Occidental, Mexico. Geomorphology, 55: 235-247.

Paganelli, F., Grunsky, E.C., Richards, J.P., and Pryde, R. 2003. Use of RADARSAT-1 principal component imagery for structural mapping. A case study in the Buffalo Head Hills, northern central Alberta, Canada. Canadian Journal of Remote Sensing, 29, no. 1: 111-140.

Pazzaglia, F.J. 2003. Landscape evolution models. Developments in Quaternary Science. Vol. 1. pp. 247-274.

Sklar, L.S. and Dietrich, W.E. 2001. Sediment and rock strength controls on river incision into bedrock. Geology, 29, no. 12: 1087-1090.

Snyder, N. P., Whipple, K.X., Tucker, G.E., and Merritts, D.J. 2000. Landscape response to tectonic forcing: Digital elevation model analysis of stream profiles in the Mendocino triple junction region, northern California. Geological Society of America Bulletin, 112, no. 8: 1250-1263.

Stea, R.R., and Kennedy, C.M. 1998. Surficial Geology of Bridgetown (NTS sheet 21A/14). Nova Scotia Department of Natural Resources Minerals and Energy Branch, Halifax, N.S. OFM 1998-002.

Stea, R.R. and Mott, R.J. 1998. Deglaciation of Nova Scotia: Stratigraphy and Chronology of Lake Sediment Cores and Buried Organic Sections. Geographie physique et Quaternaire, 50, no. 1: 3-21.

Stock, J.D., Montgomery, D. R, Collins, B.D., Dietrich, W.E., and Sklar, L. 2005. Field measurements on incision rates following bedrock exposure: Implications for process controls on the long profiles of valleys cut by rivers and debris flows. Geological Society of America Bulletin. 117: 174-194.

Stock, J. and Montgomery, D. R. 1999. Geologic constraints on bedrock river incision using the stream power law. Journal of Geophysical Research, 104, no. B3: 4983-4993.

Tague, C. and Grant, G.E. 2004. A geological framework for interpreting the low-flow regimes of Cascade streams, Willamette River basin, Oregon. Water resources Research, 40: W04303.

Toutin, T, Rivard, B. 1995. A New Tool for Depth Perception of Multi-Source Data. Photogrammetric Engineering & Remote Sensing, 61, no. 10: 1209-1211.

Turcotte, D. 1992. Fractals and Chaos in geology and geophysics. Cambridge Press, pp. 199.

Webster, T., Templin, A., Ferguson, M., Dickie, G. 2009. Remote Predictive Mapping of Aggregate Deposits using LiDAR. Canadian Journal of Remote Sensing. Vol. 35, Suppl. 1 (Special Issue on Remote Predictive Mapping), pp. S154-S166.

Webster, T., Murphy, J.B., Quinn, D. 2009. Remote Predictive Mapping of a Potential Volcanic Vent Complex in the Southern Antigonish Highlands using LiDAR, Magnetics, & Field Mapping. Canadian Journal of Remote Sensing. Vol. 35, No. 5, pp. 486-495.

Webster, T.L., Murphy, J.B., Gosse, J.C., and Spooner, I. 2006. The Application of LIDAR-derived DEM analysis for geological mapping: An Example from the Fundy Basin, Nova Scotia, Canada. Canadian Journal of Remote Sensing, Vol. 32. No. 2, pp. 173-193.

Webster, T.L., Murphy, J.B., and Gosse, J.C. 2006A. Mapping Subtle Structures with LIDAR: Flow Units and Phreomagmatic Rootless Cones in the North Mountain Basalt, Nova Scotia. Canadian Journal of Earth Sciences. Vol. 43, pp. 157-176.

Wehr, A., and Lohr, U. 1999. Airborne laser scanning—an introduction and overview, ISPRS Journal of Photogrammetry and Remote Sensing, 54, no. 2-3: 68-82.

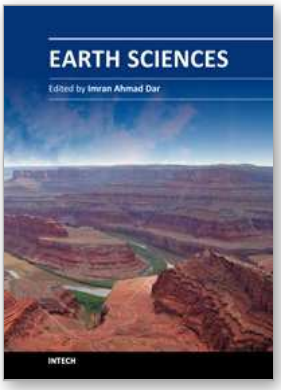

Earth Sciences
Edited by Dr. Imran Ahmad Dar

ISBN 978-953-307-861-8
Hard cover, 648 pages
Publisher InTech
Published online 03, February, 2012
Published in print edition February, 2012

The studies of Earth's history and of the physical and chemical properties of the substances that make up our planet, are of great significance to our understanding both of its past and its future. The geological and other environmental processes on Earth and the composition of the planet are of vital importance in locating and harnessing its resources. This book is primarily written for research scholars, geologists, civil engineers, mining engineers, and environmentalists. Hopefully the text will be used by students, and it will continue to be of value to them throughout their subsequent professional and research careers. This does not mean to infer that the book was written solely or mainly with the student in mind. Indeed from the point of view of the researcher in Earth and Environmental Science it could be argued that this text contains more detail than he will require in his initial studies or research.

INTECH
open science | open minds

InTech Europe
University Campus STeP Ri
Slavka Krautzeka 83/A
51000 Rijeka, Croatia
Phone: +385 (51) 770 447
Fax: +385 (51) 686 166
www.intechopen.com

InTech China
Unit 405, Office Block, Hotel Equatorial Shanghai
No.65, Yan An Road (West), Shanghai, 200040, China
中国上海市延安西路65号上海国际贵都大饭店办公楼405单元
Phone: +86-21-62489820
Fax: +86-21-62489821